THE ASTROPHYSICAL JOURNAL, 261:228–250, 1982 October 1

CIRCINUS X-1: X-RAY OBSERVATIONS WITH *SAS 3*[1]

RICHARD G. DOWER, HALE V. BRADT, AND EDWARD H. MORGAN
Department of Physics and Center for Space Research Massachusetts Institute of Technology
Received 1981 October 8; accepted 1982 April 5

ABSTRACT

Eight observations of Cir X-1 with *SAS 3*, each lasting 1–6 days, have yielded a variety of new phenomena, *viz.*, a luminous ($\sim 3 \times 10^{38}$ ergs s^{-1}, 1–20 keV, for a 10 kpc distance) state of steady emission, rapid large-intensity dips (decreases by factors of 2–4 for 3–300 s), an extremely rapid X-ray transition ($\sim 6.2 \times 10^{38}$ ergs s^{-1} to $\sim 1.3 \times 10^{38}$ ergs s^{-1} within 1 minute), and bright flares (factor of 7 increases lasting 3–20 s). Thorough searches for periodic X-ray pulsations were carried out on data trains of duration up to 6 days; upper limits for pulsations with periods greater than 250 μs range down to 0.3%. Aperiodic variability with characteristic times of 0.4–1.0 s was observed but is not well characterized by a simple shot noise model. No millisecond bursts were observed during 4×10^4 s in three separate observations. Spectral parameters derived before and after several X-ray transitions indicate that the transitions are not due to absorption of X-rays by intervening gas. Models previously proposed for the Cir X-1 system do not easily provide explanations for all the complex phenomena reported herein.

Subject headings: stars: individual — X-rays: binaries

I. INTRODUCTION AND SUMMARY

Circinus X-1 is one of the most highly variable X-ray sources known. Its rapid aperiodic variability is in many ways similar to that of Cyg X-1, the well-known black hole candidate (Oda 1977). Cir X-1 varies significantly on time scales of tenths of seconds (Jones *et al.* 1974) and occasionally milliseconds (Toor 1977). Large variations over times of hours and days have been observed (Jones *et al.* 1974; Canizares, Li, and Clark 1974; Davison and Tuohy 1975; Wilson and Carpenter 1976*a*; Buff *et al.* 1977). The long term behavior of Cir X-1 was clarified by the discovery (Kaluzienski *et al.* 1976) of a $16\overset{d}{.}6$ period between abrupt (<100 minute) transitions from high to low X-ray intensity.

At 3–6 keV, the $16\overset{d}{.}6$ cycle was characterized during 1975–1977 by an abrupt (<100 minutes) flux decrease, $\sim$12 days at low intensity, and an increase to high intensity for the 2–6 days before the next transition (Kaluzienski *et al.* 1976). Recovery to high X-ray intensity $\lesssim 1^d$ after transition has been observed in 1972 May (Jones *et al.* 1974), 1977 September (Kaluzienski and Holt 1977*c*; observation V of this work), 1978 January and February (Kaluzienski and Holt 1978), and 1979 January (Kaluzienski and Holt 1979). Year to year variations in the average light curve are apparent in data from *Ariel 5* (Murdin *et al.* 1980). Flux variations at higher energies are much less pronounced than those in the 2–6 keV band (Coe, Engel, and Quenby 1976; Buff *et al.* 1977). Consequently, the X-ray spectrum is generally steeper during periods of high intensity. Several different sets of spectral parameters have been reported (Margon *et al.* 1971; Canizares, Li, and Clark 1974; Davison and Tuohy 1975; Baity, Ulmer, and Peterson 1975; Wilson and Carpenter 1976*a*). Cir X-1 has been in active states and very low intensity ("OFF") states for hundreds of days at a time.

The radio counterpart (proposed by Clark, Parkinson, and Caswell 1975) and the emission-line optical counterpart (proposed by Mayo, Whelan, and Wickramasinghe 1976) of Cir X-1 were conclusively identified with the X-ray source (Whelan *et al.* 1977) on the basis of (1) a $\sim 1''$ positional coincidence of the star and radio source within available small X-ray error regions and (2) the occurrence of radio outbursts shortly after expected X-ray transition times. The star is located in the intersection of small X-ray error regions determined by *Uhuru* (Jones *et al.* 1974), *Ariel 5* (Wilson and Carpenter 1976*b*), *SAS 3* (Bradt *et al.* 1977), and *HEAO 1* (Gursky *et al.* 1978). The optical counterpart of Cir X-1 is faint and red ($B \approx 22$, $R \approx 16$, $K \approx 7.7$ mag; Whelan *et al.* 1977; Glass 1976). Extremely strong Hα emission provides over half the flux in the R ($\sim$6300–6800 Å) band and is variable in intensity by at least a factor of 2 (Whelan *et al.* 1977). A lower limit for the distance to the source, based on radio measurements, is 8 kpc (Goss and Mebold 1977). A distance of 10 kpc is adopted for use in this work.

The radio, infrared, and optical fluxes from Cir X-1 increase within 1–3 days (longer delays for longer wavelengths) after the *predicted* time of the transition to low X-ray flux (Whelan *et al.* 1977; Glass 1978; Hayes *et al.* 1978). The X-ray decrease and subsequent increase at longer wavelengths in the same $16\overset{d}{.}6$ cycle were observed on at least three occasions. After the X-ray transition of 1976 December 12.9 (present work), a radio flare at 21 cm began on December 14, peaked on December 17, and then faded through December 19 (Goss and Mebold 1977). At 75 cm, this flare began on

[1] This work was supported in part by NASA contract NAS5-24441.

December 15 and peaked on December 21 (Whelan *et al.* 1977). Fifteen hours after the X-ray transition of 1977 September 5.1 (Kaluzienski and Holt 1977*b*), an infrared increase from $K(2.2\ \mu m) = 10$ to $K = 7.2$ occured during ~ 3 hours (Glass 1978). An X-ray transition on 1978 January 31 was followed by a 6 cm radio flare which began on February 1 and peaked on February 3 (Murdin *et al.* 1980).

Infrared observations indicate a steady decline from the peak value by a factor of ~ 3 in 10 days with no change in colors over the *J*, *M*, *K*, and *L* bands (Glass 1978). Radio flares at one frequency with two (Haynes *et al.* 1978) and three (Thomas *et al.* 1978) peaks have been observed after the predicted X-ray transition times. The radio flare peaks were separated by ~ 1 day. The radio fluxes peaked later at longer wavelengths over the range 3–75 cm (Whelan *et al.* 1977; Haynes *et al.* 1978). After the peaks, the radio flux diminished gradually in one to several days. The quiescent radio spectrum of the source is a power law ($S \propto \nu^{\alpha}$) with $\alpha = -0.5$ and a flux of 0.2 Jy at 5 GHz (Whelan *et al.* 1977; Haynes *et al.* 1978). The source is sometimes quiescent at radio and infrared energies for long periods (Glass 1979; Nicolson, Feast, and Glass 1980), apparently coincident with sustained X-ray OFF states (Kaluzienski and Holt 1979).

The observations reported here were designed to examine in detail the variability of the X-ray intensity and spectrum of Cir X-1. This was accomplished with the continuous pointing capability of the *SAS 3* satellite X-ray observatory. On eight occasions between 1976 October and 1978 August the 1°.7 FWHM tube detectors and the 1° × 32° and 0°.5 × 32° FWHM slat detectors were pointed at Cir X-1 for periods of 1–6 days. Each observation (except Observation IV) included one of the $16^{d}.6$ X-ray transitions of the source. Data over the energy range 1–55 keV were obtained. However, Cir X-1 was never above our detector threshold in the 30–55 keV range. Time resolution of the data is 0.13 ms, 1.0 ms, 0.41 s, or 0.83 s. The data show a wide variety of spectral and intensity states, including several not previously observed.

The significant results include the following:

1. Cir X-1 exhibited a variety of spectral states with low energy cutoffs from 1.3 to 6.4 keV (for power law energy spectra) and spectral indices α ($S \propto \nu^{\alpha}$) from +0.3 to −4.4. The intensity maxima before transition were usually characterized by large fluxes at low energy (1–6 keV) and steep spectral slopes ($\alpha \sim -3.5$).

2. Though the intensity drop at the $16^{d}.6$ transition was as much as a factor of 10, Cir X-1 remained above detector threshold in the 1.2–12 keV band ($\gtrsim 1 \times 10^{36}$ ergs s^{-1} for $d = 10$ kpc) immediately following each observed transition and for up to $4^{d}.5$ afterward.

3. Three distinct types of behavior were observed for the first time: (i) a bright (3×10^{38} ergs s^{-1} for $d = 10$ kpc in the 1–20 keV band) state of steady emission and constant spectrum lasting $\gtrsim 19$ hours, (ii) intensity dips (two lasting 4 hours and one lasting 5 minutes) correlated with increases in the column density spectral parameter and several brief intensity dips (factors of 2–4 decreases for 3–300 s) with little or no spectral evolution, and (iii) bright flares (factor of 7 increases in the 1.2–12 keV band lasting 3–20 s) with little or no spectral evolution and total energies of up to 1×10^{40} ergs.

4. Two of the $16^{d}.6$ transitions were extremely rapid. The luminosity (1–20 keV, $d = 10$ kpc) decreased by a factor of 3 from a peak of $\sim 2 \times 10^{38}$ ergs s^{-1} within 2 minutes on 1976 October 24 and by a factor of 5 from a peak of $\sim 6 \times 10^{38}$ ergs s^{-1} within 1 minute on 1977 September 21.

5. Upper limits (99.9% confidence) for the percentage power in periodic X-ray pulsations range down to 1.6% for 0.25–1000 ms, 0.3% at 2 s, 1.5% at 300 s, and 23% at 10^{4} s.

6. The ~ 0.5 s aperiodic variability of Cir X-1 is *not* well characterized by a simple shot noise model. The characteristic time of the variability is usually in the range 0.4–1.0 s. In one orbit when Cir X-1 was in a hard spectral state after the 1977 September 21 transition, a characteristic time of ~ 20 ms was observed.

7. No millisecond bursts were detected during observations in 1977 May (10^{4} s), 1978 June (10^{4} s), or 1978 August (2×10^{4} s). Millisecond bursts previously reported by us (Dower, Bradt, and Canizares 1977) from the 1977 January observation are now believed to be spurious.

II. DATA ACQUISITION

The observation times were chosen to include the $16^{d}.6$ transitions and the few days before each transition when Cir X-1 was expected to be relatively bright (Kaluzienski *et al.* 1976). The observations lasted 0.8–6 days, with the most extensive coverage 1977 September 20–October 11 during which two transitions and $\sim 50\%$ of the intervening $16^{d}.6$ cycle were observed. The primary detection systems used were those with tubular collimators (1°.7 FWHM circular fields of view) with argon-filled (~ 80 cm^2 effective area and 1.2, 2.8, 5.6, 12 keV energy boundaries) and xenon-filled (~ 115 cm^2 effective area and 8, 19, 30, 39, 55 keV energy boundaries) proportional counters (Lewin *et al.* 1976*b*). Data from the 1.6–15 keV energy channels of the 1° × 32° FWHM center slat collimator detector (75 cm^2) and 0°.5 × 32° FWHM right slat collimator detector (75 cm^2: Buff *et al.* 1977) were usually combined with the 1.2–12 keV data from the argon tube detector for the 1 ms and $\frac{1}{8}$ ms time resolution observations.

Two satellite telemetry modes were used. In mode A, X-ray events from all detectors are read into the telemetry stream with time resolution of 0.416 s or 0.831 s. In mode B, X-ray events from a selected energy channel or group of channels are accumulated in the 4096-bit high-speed event monitor (HSEM) (Ulmer *et al.* 1977; Primini 1976). The 4096-bit memory of the HSEM is filled sequentially at a selected sampling rate of $\frac{1}{8}$, 1, or 8 ms per bit. Each bit represents zero counts or ≥ 1 counts. During the ~ 6 s following accumulation, the data are read out of the memory into the telemetry

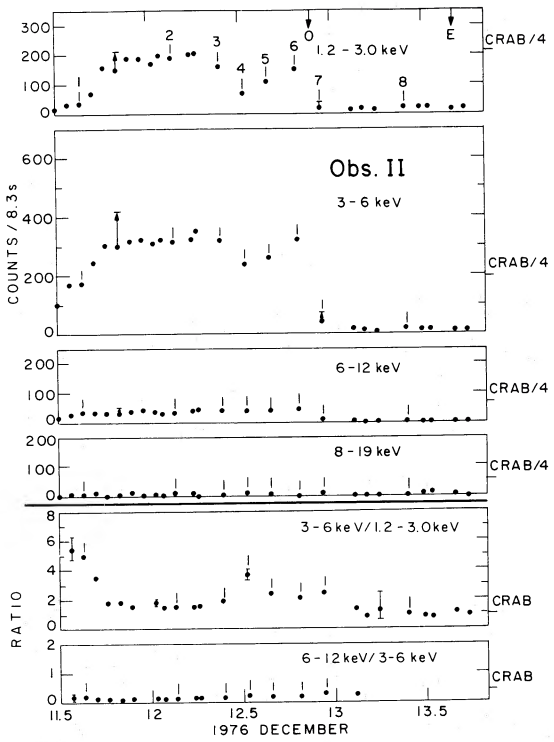

FIG. 1a

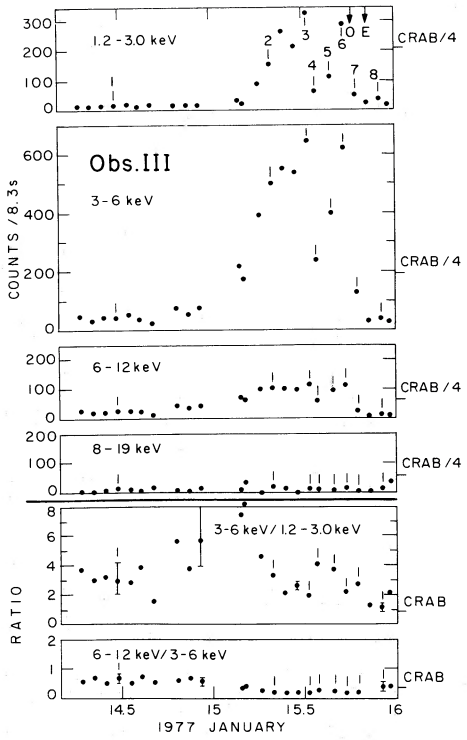

FIG. 1b

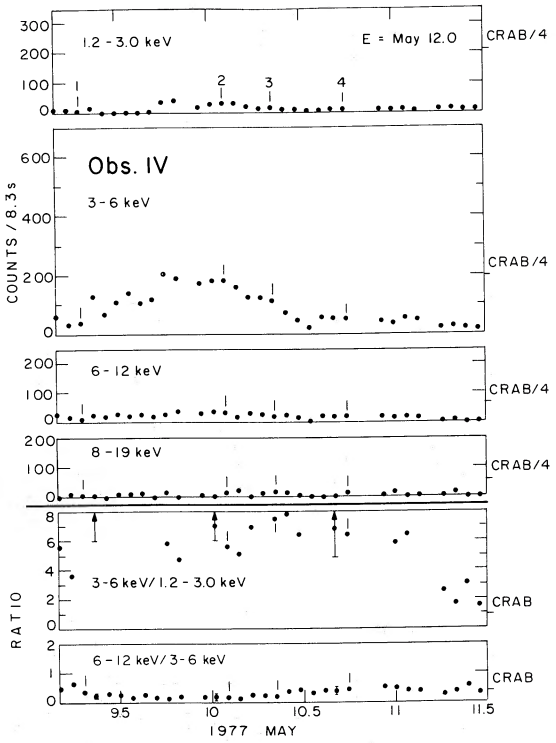

FIG. 1c

FIG. 1.—(*a*) Observation II counting rates and ratios of rates. The rates are obtained from ~5 min samples once each orbit near an immersion into, or emersion from, Earth occultation. The background rate obtained from the nearby occultation has been subtracted. The rates are not corrected for the position of the source in the collimator fields of view for this one observation due to limited aspect. The maximum corrections for aspect are indicated by arrows. (The rates *are* corrected for aspect in Figs. 1*b*–*g*.) For a source with the spectrum of the Crab Nebula, 1 count per 8.3 s corresponds to flux densities of 2.7, 1.5, 2.3, and 1.8 μJy (averaged over the bandwidth) for the 1.2–3, 3–6, 6–12, and 8–19 keV channels, respectively. The corresponding luminosities at 10 kpc, again for 1 count per 8.3 s, are 1.4×10^{35}, 1.2×10^{35}, 4.0×10^{35}, and 5.6×10^{35} ergs s^{-1}. Counting rates equal to one-quarter the rate of the Crab Nebula are indicated on the plots. Observed times (O) of the beginnings of the declines which define the transitions are marked by arrows at the tops of the plots. Expected transition times (E, Kaluzienski and Holt 1977*a*) are also indicated. Data used for spectral calculations are labeled with ID numbers from Table 2. The increase in flux (~Dec 11.7) and the long dip (~Dec 12.6) may be due to changing absorption. The transition (Dec 12.9) does not follow this pattern. (*b*) Observation III counting rates and ratios. In this case the large enhancement is fitted (Table 1) with a steepening spectrum, the long dip by an increase in the absorption parameter, and the final decrease by only modest spectral changes. See Fig. 1*a* legend. (*c*) Observation IV counting rates and ratios. The gradual decline precedes the expected transition time by ~$1^d.8$. The spectrum is highly cut off and very steep during the high intensity state. Compare the low 1–3 keV flux to observations II and III. Also see legend to Fig. 1*a*.

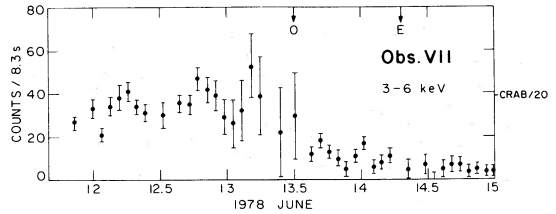

FIG. 1*f*

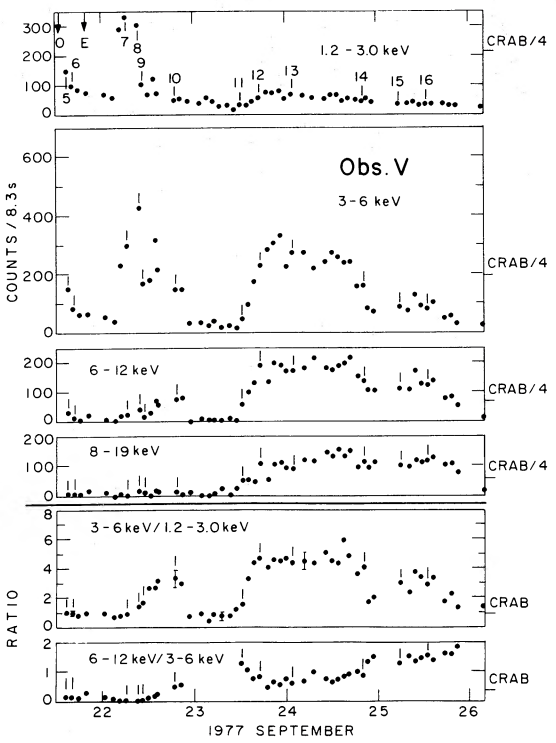

FIG. 1*d*

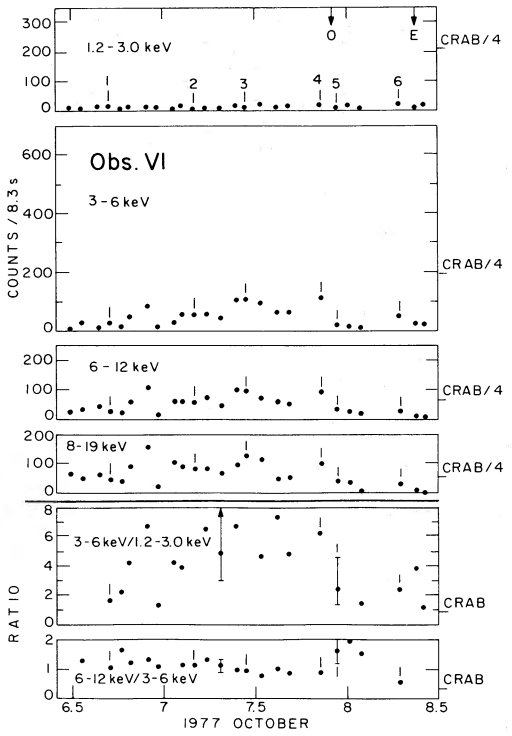

FIG. 1*e*

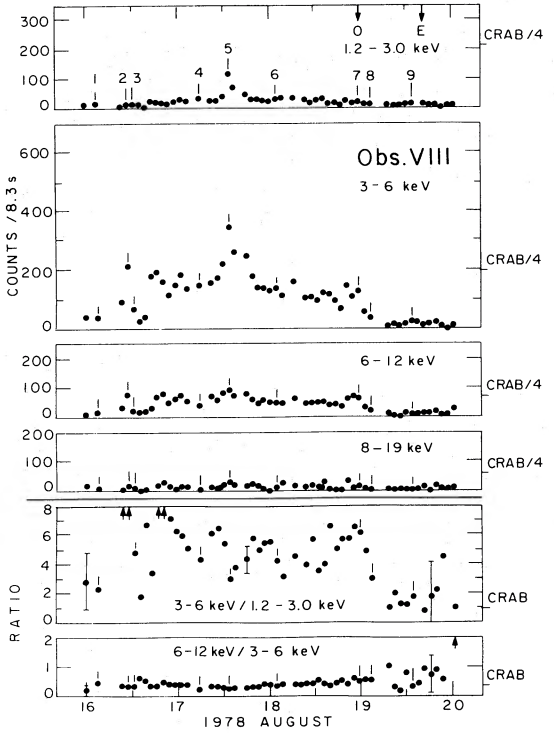

FIG. 1*g*

FIG. 1.—(*d*) Observation V counting rates and ratios for the posttransition portion of the observation. Note the intense flare and the high sustained 8–19 keV flux. The pretransition fluxes would exceed the scales shown here for the lower energy channels, viz., 1700, 2300, and 250 cts per 8.3 s for the 1.2–3, 3–6, 6–12 keV channels, respectively (see Figs. 4*a*, *b*). See also legend to Fig. 1*a*. (*e*) Observation VI counting rates and ratios. Note that the 8–19 keV flux is unusually high. See also legend to Fig. 1*a*. (*f*) Observation VII counting rates for 3–6 keV channel. The source was at a very low luminosity and visible only in the 3–6 keV channel. See also legend to Fig. 1*a*. (*g*) Observation VIII counting rates and ratios. Again note the low 1–3 keV flux. Spectral fits yielded a very steep ($\alpha = -4.4$, $S \propto \nu^{\alpha}$) and highly cutoff spectral shape for the first flare (Aug 16.4), then a relatively constant shape with moderate slope ($\alpha = -2.6$) until the transition, and finally some hardening (to $\alpha = -1.7$). See also legend to Fig. 1*a*.

stream and no new data are obtained. Then the memory is reset and accumulation begins again.

The dates, primary data modes, and quality of the satellite aspect solution for the eight observations of Cir X-1 are listed in Table 1. For orbits when star data are available, typically during the nighttime portion of each orbit, the aspect solution is accurate to $\sim 1'$. During sunlit portions of those orbits, we estimate aspect by interpolation to an accuracy of $\lesssim 3'$. For Observations III–VIII, stellar aspect solutions are available for much of every orbit. For Observations I and II (1976 October and December), stellar aspect solutions were obtained at only about one point in each orbit due to the proximity of the Sun to Cir X-1. (The star camera was coaligned to the X-ray detectors.) For Observations I and II, aspect solutions accurate to $\lesssim 0.^\circ 3$ were interpolated between star solutions by using values of the commanded spin rates and average spin-axis drift rates. During the mode B (HSEM) orbits of Observations III, IV, VII, and VIII more than 100 s of both on-source and background data were obtained in mode A (to observe the spectrum of the source) as Cir X-1 entered or emerged from Earth occultation. Some of the significant results of each observation are also listed in Table 1.

III. X-RAY LIGHT CURVES AND SPECTRA

The X-ray light curves vary from cycle to cycle of the $16^d.6$ period. This was indicated by the data of Kaluzienski *et al.* (1976) and is evident from our observations. To illustrate this variability, we present summaries of intensity variations and spectral hardness ratios from Observations II-VIII in Figures 1*a*–1*g* and higher time resolution plots in Figures 2–6. The intensity points in Figure 1 were obtained once per orbit (~ 95 minutes) from 83 s averages of observed fluxes. These averages were usually taken immediately before or after Earth occultation of the source to facilitate background subtraction. Short-duration flares and intensity dips in the source as well as regions of background enhancement due to the South Atlantic Anomaly or the Earth's soft X-ray albedo were avoided.

TABLE 1

SAS 3 CIRCINUS X-1 POINTED OBSERVATION SUMMARY

Obs.	Dates	Data Modes[a]	Comments[b]
I	1976 Oct 24.8–25.6	A, 12 orbits[c] B(1 ms), 2 orbits	Few star aspect points. Aspect interpolated to $\sim 0.^\circ 3$. Possible absorption event.
II	1976 Dec 11.4–13.7	A, 27 orbits B(1 ms), 6 orbits B($\frac{1}{8}$ ms), 3 orbits	Maximum point offset from Cir X-1 $0.^\circ 8$. Aspect interpolated 6 orbits to $\lesssim 0.3$. 0.5–1.0 s aperiodic variability.
III	1977 Jan 13.8–16.0	A, ... B(1 ms), 7 orbits B($\frac{1}{8}$ ms), 25 orbits	Mode A at immersion, during Earth occultation and at emersion. Maximum pointing offset $1.^\circ 0$, 1′–3′ aspect.
IV	1977 May 9.1–11.5	A, ... B(1 ms), 8 orbits B($\frac{1}{8}$ ms), 28 orbits	Mode A at immersion. Maximum pointing offset $0.^\circ 5$, 1′–3′ aspect. Atypical early intensity decline. No millisecond bursts.
V	1977 Sep 20.6–26.6	A, 72 orbits B(1 ms), 6 orbits	Maximum pointing offset $0.^\circ 7$, 1′–3′ aspect. Repeated scans across source when intensity low. Intensity dips, rapid transition, large flares.
VI	1977 Oct 5.3–11.0	A, 81 orbits B(1 ms), 1 orbit	Maximum pointing offset $0.^\circ 7$, 1′–3′ aspect. Repeated scans across source when intensity low; Hard source spectrum.
VII	1978 Jun 11.6–15.6	A, 10 orbits B(1 ms), ... B($\frac{1}{8}$ ms), 52 orbits	Mode A at emmersion during Mode B orbits. Maximum pointing offset $1.^\circ 7$, 1′–3′ aspect. Source faint. No millisecond bursts.
VIII	1978 Aug 14.0–20.2	A, 1 orbit B(1 ms), 5 orbits B($\frac{1}{8}$ ms), 75 orbits	Mode A at immersion. Maximum pointing offset $1.^\circ 0$, 1′–3′ aspect. No millisecond bursts.

[a] Mode A data (1.2–55 keV) have 5 channel energy resolution, and 0.416 s time resolution (1.2–6 keV) or 0.83 s time resolution (6–55 keV). Mode B data have 1 channel (usually 1.2–15 keV) energy resolution and $\frac{1}{8}$ ms, 1 ms, or 8 ms time resolution.

[b] For most of each observation the pointing accuracy was substantially better than the maximum excursions given here. A $0.^\circ 85$ excursion results in reduction of effective detector area by $\frac{1}{2}$ in the $1.^\circ 7$ FWHM tubular collimator systems.

[c] Each mode A orbit contains ~ 4000 s of unocculted data.

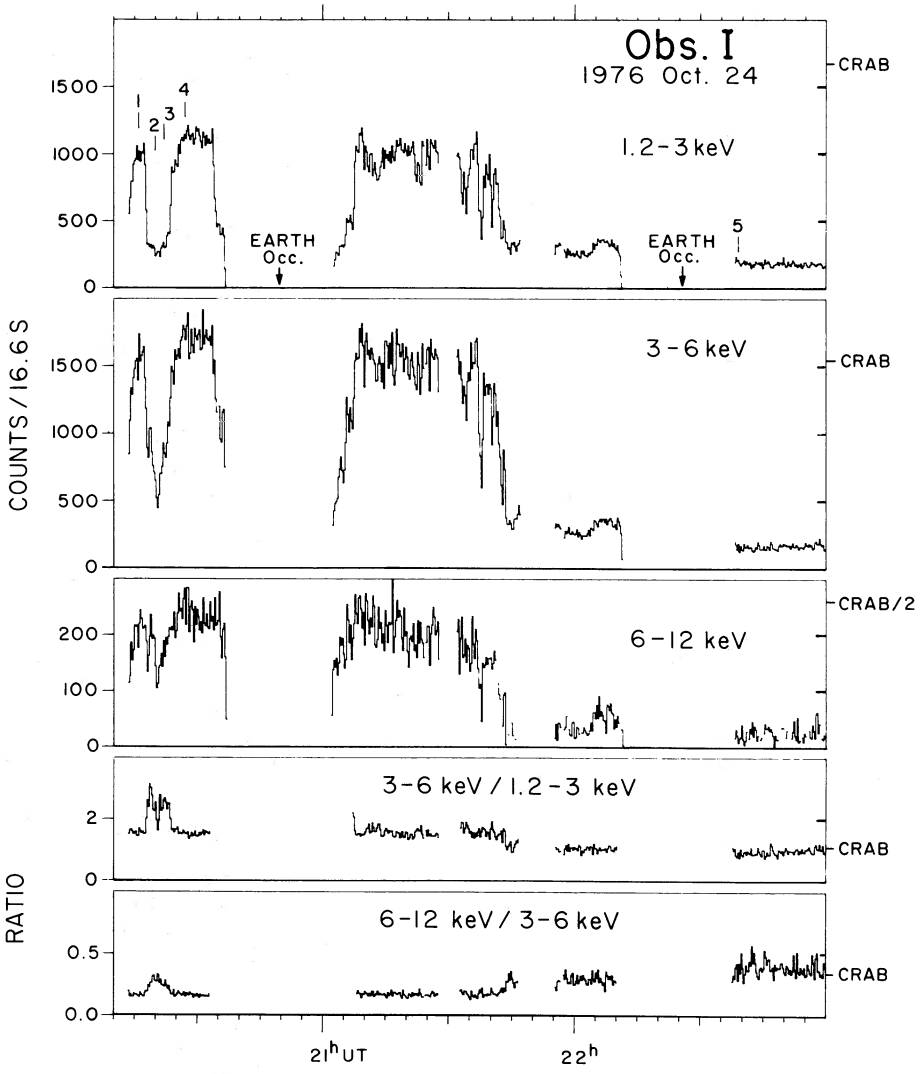

FIG. 2.—Observation I transition. Background is subtracted, and data are corrected for source position in collimator field of view. Spectra were calculated (Table 2) for the times (1–5) indicated. Note the spectrally complex intensity dip at $20^h\ 20^m$ and the rapid relatively color-independent pretransition dips.

The background was measured during Earth occultation within ~800 s of the corresponding intensity measurement. The uncertainty due to background subtraction is $\lesssim 5$ counts per 8.3 s in any channel. After background subtraction, the data (except for Observation II with its larger aspect uncertainty) were corrected for source position in the collimator fields of view with star aspect accurate to ~1′–3′. The combined errors due to counting statistics, background uncertainty and aspect uncertainty (except Fig. 1*a* Observation II) are $\lesssim 10$ counts per 8.3 s, i.e., less than the size of the plotted points (except Fig. 1*f*, Observation VII).

Observation I was so short that it is not plotted in Figure 1. It is discussed below (see Fig. 2). In Figure 1*d*, only the posttransition data of Observation V are shown. The pretransition fluxes exceeded the scales of Figure 1 by an order of magnitude (see Fig. 4). For Observation VI (1977 Oct. 5.3–11.0), Cir X-1 was above our detector thresholds only during October 6.5–8.4 (Fig. 1*e*). During Observation VII, Cir X-1 was visible only in the 3–6 keV channel (Fig. 1*f*). Satellite difficulties interrupted the first two days of Observation VIII, so only the portion after 1978 August 16 is plotted (Fig. 1*g*).

The expected (E, Kaluzienski and Holt 1977*a*) and observed (O) transition times are indicated in Figures 1*a*–1*g*. The transition times of Observations I, III, and V are consistent with the revised ephemeris of Kaluzienski and Holt (1977*a*): $T(\mathrm{JD}) = 2{,}443{,}292.118(\pm 0.09) + n(16.595 \pm 0.004)$, where T is the time for the abrupt transition from high to low flux (3–6 keV), n is an integer, and $n = 0$ corresponds to 1977 May 28.618. The

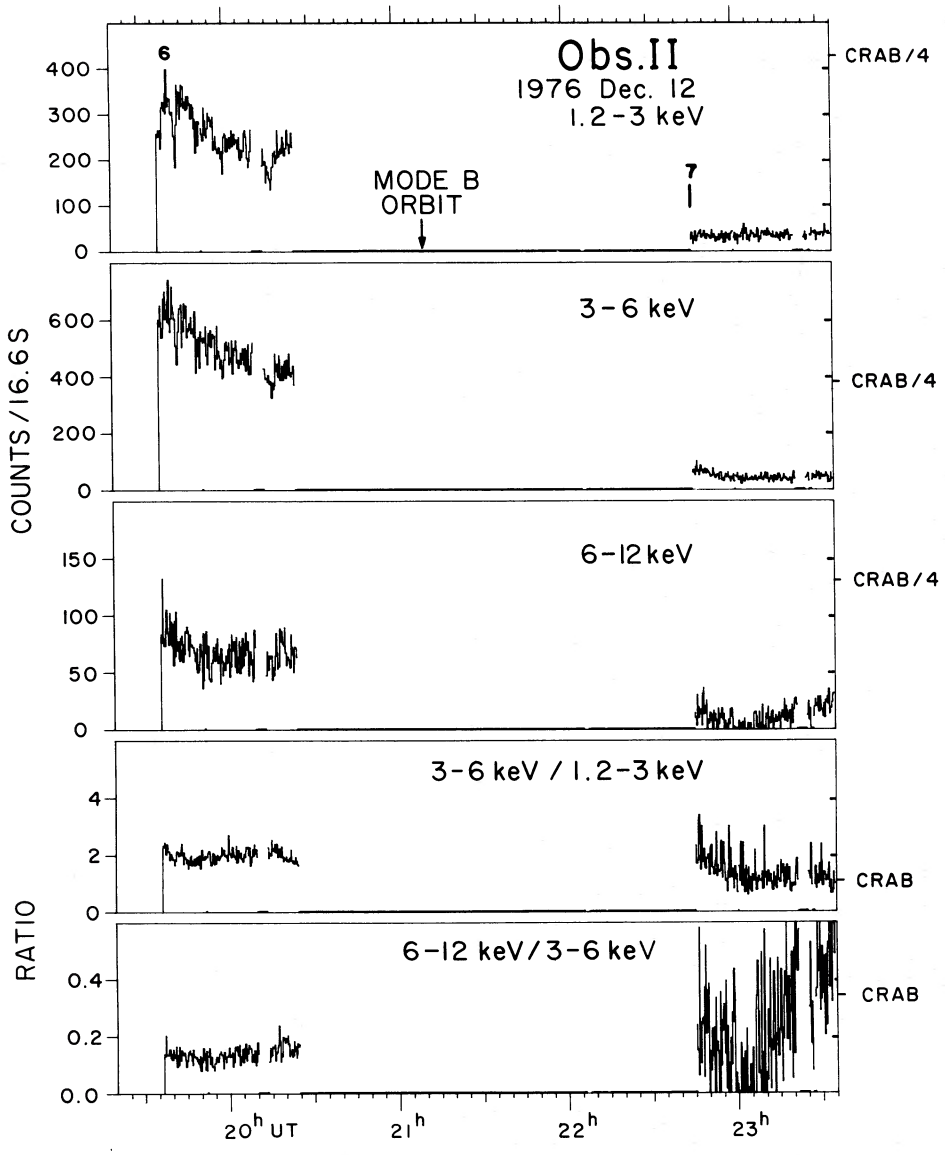

FIG. 3.—Observation II transition. Background is subtracted and aspect corrections are applied.

transitions of Observations II, VI, VII, and VIII occurred $0^d.8$, $0^d.4$, $0^d.8$, and $0^d.7$, respectively, earlier than expected. It should be noted that the peak 3–6 keV flux before transition in those observations was $S \lesssim S_{\text{Crab}}/4$, in contrast to the $S \gtrsim S_{\text{Crab}}$ 3–6 keV fluxes before the transitions used to determine the ephemeris of Kaluzienski and Holt. The intensity decline in Observation IV on May 10 is not a typical transition in that it is much more gradual ($\sim 0^d.5$) than the other Cir X-1 transitions and precedes the expected transition time by ~ 2 days. The observation was concluded $0^d.5$ before the expected transition time. Radio and optical flares were observed about 12 hours after the expected transition time on May 12 (Haynes *et al.* 1978).

The recovery to high X-ray flux levels $\lesssim 1^d$ after transition seen in Observation V and in other recent observations (Kaluzienski and Holt 1977*c*, 1978, 1979) suggests that an event observed by *Uhuru* in 1972 May (Jones *et al.* 1974) was an X-ray transition and recovery. However, that transition and another apparent transition observed by *Uhuru* in 1971 February (Forman, Jones, and Tananbaum 1976) occurred $2^d.8$ and $4^d.3$ earlier, respectively, than expected from the standard ephemeris. These differences are difficult to reconcile with the ephemeris even if the period decrease suggested by radio observations (Nicolson 1980) is taken into account. In any case, it is not unusual for individual transition times to deviate from the expected time by $\lesssim 0^d.9$.

Typical power law, thermal bremsstrahlung, and blackbody spectral parameters derived primarily from

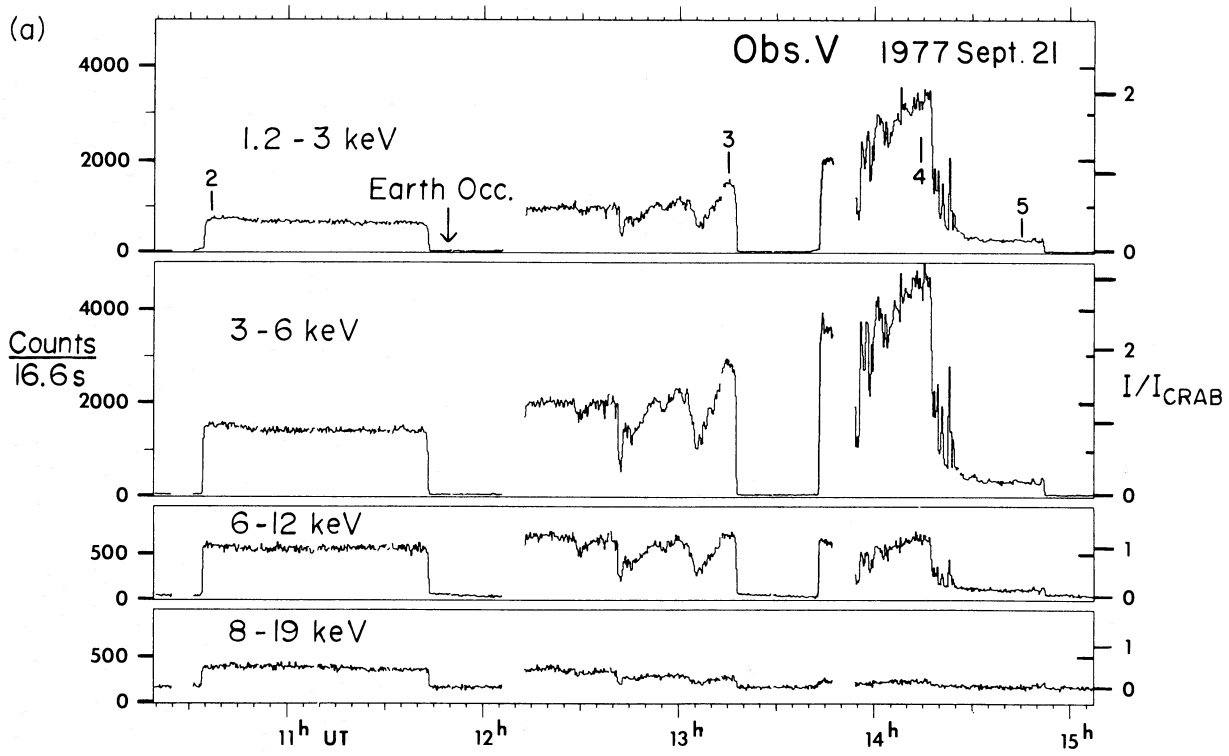

FIG. 4*a*

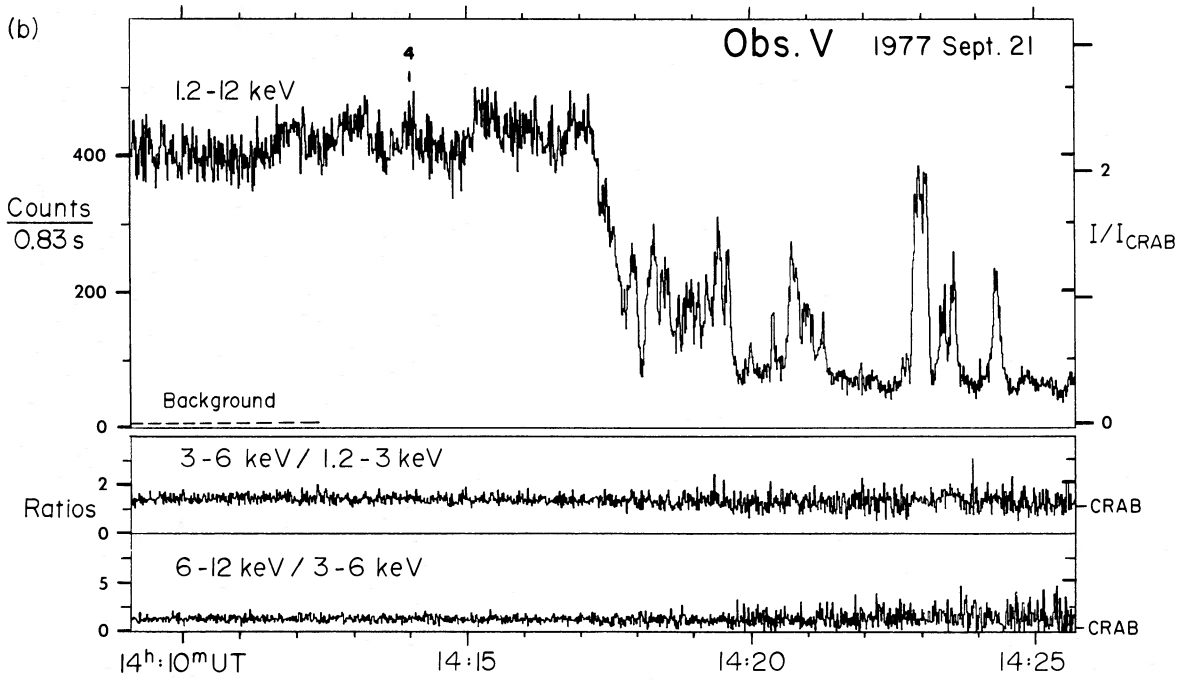

FIG. 4*b*

FIG. 4.—(*a*) Observation V transition of Cir X-1 displaying unusual steady intensity state (10:35–12:20 UT), large intensity dips (12:25–14:15 UT), rapid (~60 s) transition (14:17 UT), and bright flares after transition (14:18–14:25 UT). The source was in the steady state at least 19 hours (from Sep 20.6). Background counting rates are visible during Earth occultation. Spectra were calculated (Table 2) for the times (2–5) indicated. (*b*) Observation V transition (0.83 s resolution). Background rate during Earth occultation is indicated. Counting rate ratios were determined after background was subtracted. Note the relative constancy of the ratios during the rapid intensity changes. Compare to much larger changes for slower variations (Figs. 1*a–g*).

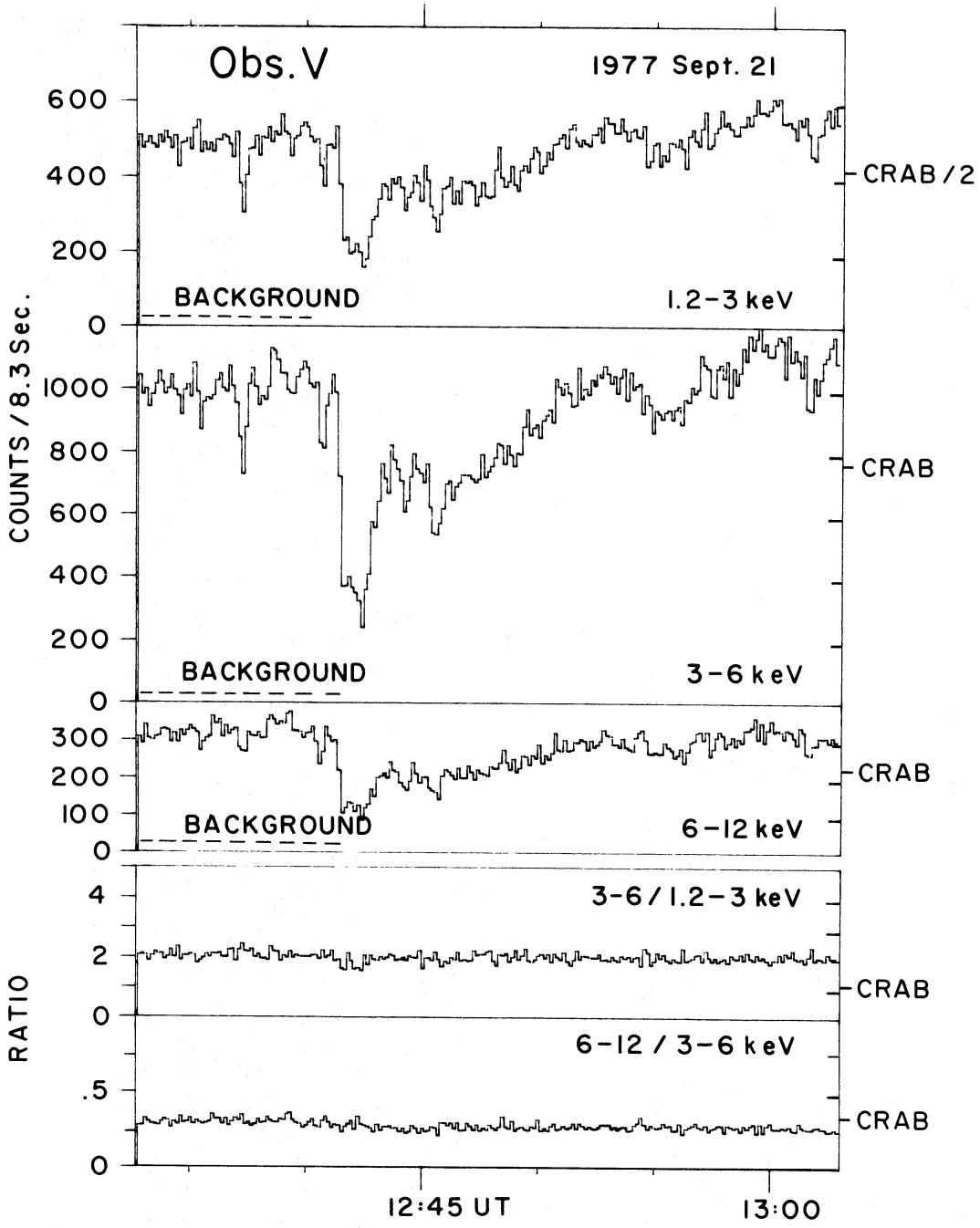

FIG. 5.—Observation V: large intensity dip before transition. Background rates during Earth occultation are indicated. Counting rate ratios were determined after subtracting background. Note the constancy of the ratios compared to the dip at 20^h20^m in Observation I (Fig. 2).

data in Figure 1 are given in Table 2. The parameters were obtained from a least-squares fit to data from 3–5 energy channels. The errors represent the extent of the 1 σ error contour for a parabolic minimum. Data points in Figure 1 used for spectral fits are identified by the appropriate spectrum number from Table 2. Light curves and spectra for each observation are discussed in detail below.

a) Observation I

Observation I lasted only a few orbits. The transition (Fig. 2) at 21:43 UT is marked by a factor of ~ 3 decrease in flux in $\lesssim 2$ minutes. Several large intensity dips and recoveries precede the transition. The large dip centered at 20:20 UT is 5 minutes long. Significant spectral changes during the large dip are apparent in

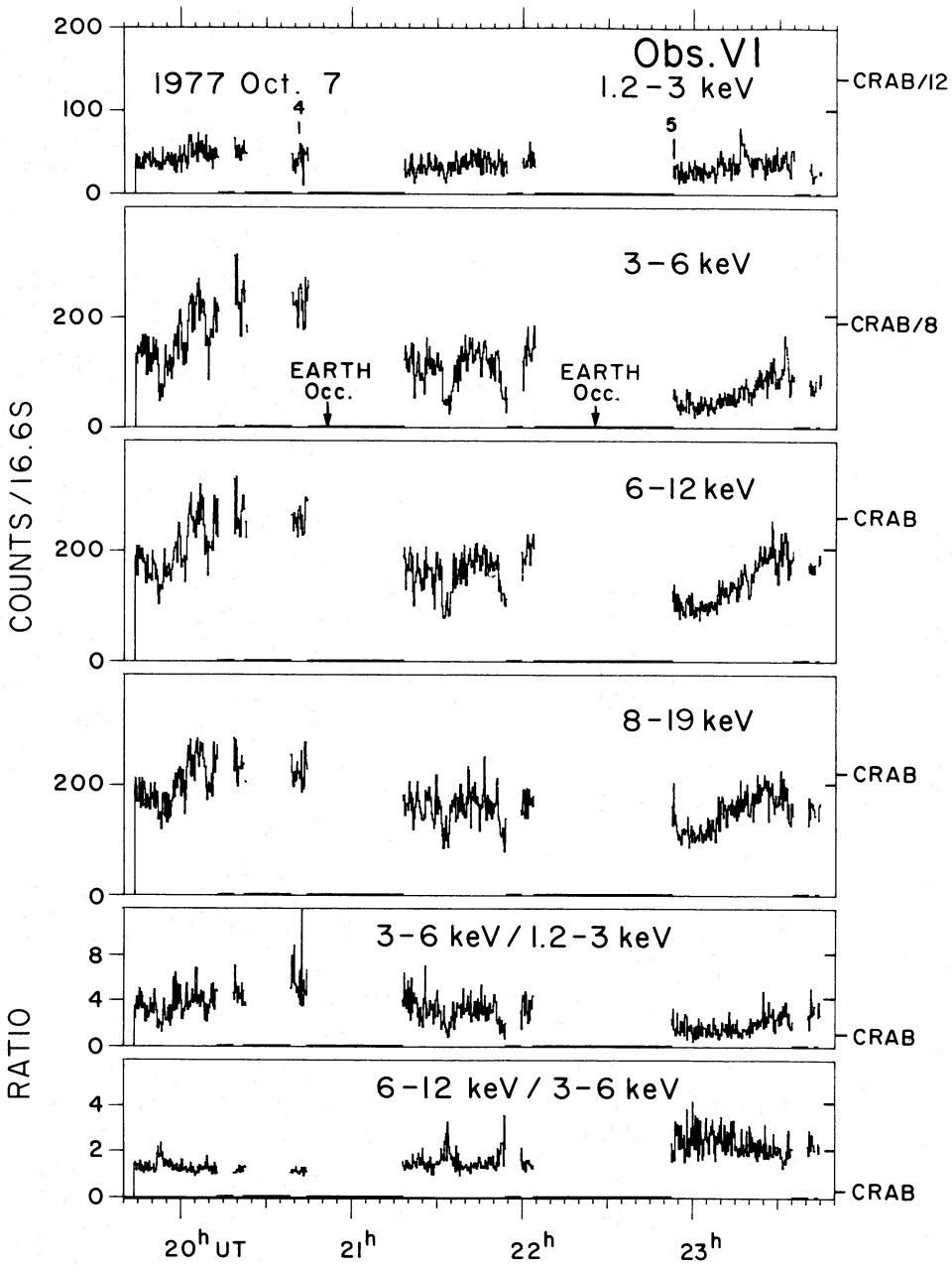

FIG. 6.—Observation VI transition. Note the large 8–19 keV flux (see Fig. 1*e*) and chaotic behavior. The transition is apparent in the factor of ~5 decrease (3–6 keV) from 20^h to 23^h. Background has been subtracted and aspect corrections applied.

Figure 2. Spectral fits were made at the times indicated ("1" to "4") in Fig. 2. The fits (I-1) to I-4 in Table 2) yield, except for the deepest portion in the center (25 s), a temporary increase of 5×10^{22} atoms cm^{-2} in the column density parameter, N_H, with no change in spectral shape. Several other more rapid intensity dips (factors of 2–3 for 10–80 s) occurred before the transition. They exhibit only a modest hardening in the counting rate ratios. The several pretransition dips approach the post-transition fluxes in each energy channel. This may suggest a two-component source. The ratios of rates during the transition show that the 3–6 keV channel decreased by a greater factor then either the 1.2–3 keV or 6–12 keV channel. Spectral fits 1 hour before and 1 hour after the transition (I-4 and I-5) indicate a decrease in the absorption parameter. After the transition there was a steady slow decline lasting $\gtrsim 2$ hours. Cir X-1 was clearly visible (at $\sim 10^{37}$ ergs s^{-1} for $d = 10$ kpc) throughout

TABLE 2

SPECTRAL PARAMETERS

Spectrum No.	Date	Time (UT)	Spectrum Type[a]	I_0 (cts cm^{-2} s^{-1} keV^{-1})	N_H[b] (10^{22} atoms cm^{-2})	E_a[c] (keV)	α or kT (keV)	DOF	χ^2	L_x (1–20 keV)[d] (10^{37} ergs s^{-1})	Comments
Observation I:											
I-1	1976 Oct 24	20:16	PL	274 ± 63[e]	9.3 ± 0.5[e]	3.2	−3.2 ± 0.1[e]	0	0.0	18.7	Before dip
			TB	19.3 ± 2.3	4.6 ± 0.3	2.5	2.0 ± 0.1	0	0.0	17.9	
			BB	1.7 ± 0.2	1.0 ± 0.2	1.4	1.01 ± 0.02	0	0.0	18.1	
I-2	24	20:20	PL	15.7 ± 9.6	6.4 ± 1.3	2.8	−2.2 ± 0.4	0	0.0	6.4	Bottom of dip
			TB	2.5 ± 0.8	3.2 ± 0.8	2.1	2.9 ± 0.5	0	0.0	5.8	
			BB	0.22 ± 0.08	0.0 ± 0.7	0	1.2 ± 0.1	0	0.2	5.7	
I-3	24	20:22	PL	246 ± 86	14.4 ± 0.9	3.7	−3.3 ± 0.2	0	0.0	10.1	During dip
			TB	14.6 ± 2.6	9.0 ± 0.6	3.1	2.0 ± 0.1	0	0.0	9.5	
			BB	1.1 ± 0.2	4.8 ± 0.6	2.5	1.03 ± 0.04	0	0.0	9.3	
I-4	24	20:27	PL	285 ± 60	8.8 ± 0.4	3.1	−3.2 ± 0.1	2	1.7	18.6	After dip and before transition
			TB	17.6 ± 2.0	4.0 ± 0.3	2.3	2.0 ± 0.1	2	9.9	18.3	
			BB	1.6 ± 0.2	0.4 ± 0.2	1.0	1.02 ± 0.02	2	19.3	18.6	
I-5	24	22:39	PL	41 ± 93	6.4 ± 3.9	2.8	−3.7 ± 1.4	2	2.3	1.9	After transition
			TB	2.1 ± 2.4	1.7 ± 2.0	1.7	1.6 ± 0.7	2	2.8	2.0	
			BB	0.5 ± 1	0.0 ± 2.9	0	0.8 ± 0.2	2	4.1	2.1	
Observation II:											
II-1	1976 Dec 11	15:15	PL	351 ± 273	21.5 ± 2.8	4.4	−3.8 ± 0.4	2	0.1	4.0	Before rise
			TB	11.4 ± 4.8	14.6 ± 2.1	3.8	1.8 ± 0.2	2	1.5	3.8	
			BB	0.8 ± 0.4	10.0 ± 2.0	3.3	1.0 ± 0.1	2	2.4	3.8	
II-2	12	03:16	PL	492 ± 310	12.3 ± 1.3	3.5	−4.1 ± 0.4	2	3.8	7.2	
			TB	17.5 ± 6.0	6.3 ± 0.8	2.8	1.5 ± 0.2	2	6.5	7.1	
			BB	1.6 ± 0.6	2.5 ± 0.7	2.0	0.9 ± 0.1	2	7.3	7.1	
II-3	12	09:34	PL	414 ± 228	13.1 ± 1.2	3.6	−3.9 ± 0.3	2	0.5	7.2	
			TB	14.9 ± 4.3	7.0 ± 0.7	2.9	1.7 ± 0.2	2	0.3	7.0	
			BB	1.3 ± 0.4	3.1 ± 0.7	2.1	0.9 ± 0.05	2	0.7	7.0	
II-4	12	12:44	PL	344 ± 215	17.8 ± 1.8	4.1	−3.7 ± 0.4	2	0.3	5.4	Bottom of long dip before transition
			TB	12.7 ± 4.3	11.4 ± 1.3	3.4	1.8 ± 0.2	2	2.9	5.1	
			BB	1.0 ± 0.4	7.0 ± 1.2	2.9	1.0 ± 0.1	2	4.4	5.0	
II-5	12	15:52	PL	407 ± 253	15.1 ± 1.5	3.8	−3.9 ± 0.4	2	0.2	6.0	
			TB	13.9 ± 4.5	8.8 ± 1.0	3.1	1.7 ± 0.2	2	0.4	5.8	
			BB	1.1 ± 0.4	4.6 ± 0.9	2.4	0.9 ± 0.1	2	1.0	5.8	
11-6	12	19:37	PL	389 ± 183	13.5 ± 1.1	3.7	−3.8 ± 0.3	2	4.9	7.3	Before transition
			TB	14.2 ± 3.4	7.3 ± 0.7	2.9	1.7 ± 0.1	2	1.0	7.1	
			BB	1.2 ± 0.3	3.3 ± 0.6	2.2	0.94 ± 0.04	2	0.4	7.1	
II-7	12	22:45	PL	2.7 ± 3.5	8.3 ± 3.6	3.1	−2.0 ± 0.7	2	5.4	1.3	After transition
			TB	0.5 ± 0.3	5.1 ± 2.6	2.5	3.3 ± 1.4	2	8.2	1.1	
			BB	0.04 ± 0.04	1.7 ± 2.5	1.7	1.3 ± 0.3	2	9.2	1.0	
II-8	13	09:47	PL	5.0 ± 24	6.3 ± 10	2.8	−3.0 ± 3.3	2	2.4	0.5	
			TB	0.6 ± 2	3.2 ± 7.1	2.1	1.7 ± 2.3	2	2.4	0.5	
			BB	0.07 ± 0.3	0.01 ± 6.7	0.3	0.9 ± 0.7	2	2.4	0.5	
Observation III:											
III-1	1977 Jan 14	11:34	PL	0.7 ± 0.4	7.2 ± 2.8	2.9	−1.0 ± 0.3	2	10.1	2.7	
			TB	0.22 ± 0.07	4.9 ± 2.1	2.5	9.5 ± 3.5	2	5.7	2.6	
			BB	0.007 ± 0.003	0.0 ± 1.7	0.0	2.2 ± 0.3	2	1.5	2.4	
III-2	14	08:01	PL	307 ± 75	15.2 ± 0.7	3.8	−3.2 ± 0.1	2	15.8	12.3	
			TB	15.3 ± 2.0	9.3 ± 0.5	3.2	2.1 ± 0.1	2	3.9	11.8	
			BB	1.1 ± 0.2	4.9 ± 0.4	2.5	1.08 ± 0.03	2	5.9	11.5	

TABLE 2—*Continued.*

Spectrum No.	Date	Time (UT)	Spectrum Type[a]	I_0 (cts cm^{-2} s^{-1} keV^{-1})	N_H[b] (10^{22} atoms cm^{-2})	E_a[c] (keV)	α or kT (keV)	DOF	χ^2	L_x (1–20 keV)[d] (10^{37} ergs s^{-1})	Comments
III-3	15	12:43	PL	268 ± 57	10.7 ± 0.5	3.4	−3.2 ± 0.1	2	23.4	16.2	6[h] before transition
			TB	15.2 ± 1.7	5.5 ± 0.3	2.6	2.2 ± 0.1	2	1.3	15.8	
			BB	1.2 ± 0.1	1.6 ± 0.3	1.6	1.07 ± 0.03	2	0.5	15.7	
III-4	15	13:47	PL	106 ± 48	16.1 ± 1.6	3.9	−3.0 ± 0.2	2	14.4	6.3	Bottom of intensity dip
			TB	6.2 ± 1.5	10.4 ± 1.1	3.3	2.4 ± 0.2	2	13.2	5.9	
			BB	0.4 ± 0.1	5.8 ± 1.1	2.7	1.2 ± 0.1	2	14.9	5.7	
III-5	15	15:51	PL	262 ± 76	16.4 ± 0.9	3.9	−3.2 ± 0.2	2	32.6	10.0	
			TB	11.9 ± 1.8	10.1 ± 0.7	3.3	2.2 ± 0.1	2	4.0	9.6	
			BB	0.8 ± 0.1	5.5 ± 0.6	2.6	1.12 ± 0.03	2	0.02	9.5	
III-6	15	17:29	PL	262 ± 54	11.3 ± 0.5	3.4	−3.2 ± 0.1	2	16.8	15.5	High intensity before transition
			TB	15.3 ± 1.6	6.0 ± 0.3	2.7	2.2 ± 0.1	2	0.02	15.0	
			BB	1.2 ± 0.1	2.1 ± 0.3	1.8	1.07 ± 0.02	2	2.4	14.8	
III-7	15	19:02	PL	38 ± 27	12.0 ± 1.9	3.5	−2.9 ± 0.4	2	4.8	3.3	After transition
			TB	2.8 ± 1.1	7.1 ± 1.3	2.9	2.4 ± 0.4	2	6.7	3.1	
			BB	0.22 ± 0.09	3.0 ± 1.2	2.1	1.1 ± 0.1	2	8.0	3.0	
III-8	15	22:10	PL	0.3 ± 0.2	0.8 ± 2	1.3	−0.9 ± 0.4	2	1.3	2.1	
			TB	0.15 ± 0.06	0.0 ± 1.0	0	7.9 ± 3.9	2	2.0	1.9	
			BB	0.08 ± 0.12	0.0 ± 2.7	0	1.0 ± 0.4	2	22.2	1.1	
Observation IV:											
IV-1	1977 May 9	07:14	PL	8 ± 16	19 ± 12	4.1	−2.3 ± 1.0	2	1.9	1.4	Before intensity increase
			TB	0.7 ± 0.8	12.9 ± 8.7	3.6	3.3 ± 1.6	2	3.1	1.3	
			BB	0.05 ± 0.06	8.5 ± 9.1	3.1	1.3 ± 0.3	2	4.0	1.2	
IV-2	10	02:07	PL	566 ± 433	23.8 ± 3.1	4.5	−4.0 ± 0.4	2	3.7	4.1	At maximum intensity before decline
			TB	16.4 ± 7.0	16.7 ± 2.4	4.0	1.6 ± 0.2	2	7.9	3.8	
			BB	1.3 ± 0.5	12.1 ± 2.3	3.5	0.9 ± 0.1	2	9.2	3.8	
IV-3	10	08:25	PL	180 ± 200	24.2 ± 4.9	4.6	−3.6 ± 0.6	2	12.5	2.8	During decline
			TB	8.9 ± 6.1	18.5 ± 4.3	4.1	1.8 ± 0.3	2	19.8	2.5	
			BB	0.8 ± 0.6	14.6 ± 4.4	3.8	0.9 ± 0.1	2	21.9	2.4	
IV-4	10	17:50	PL	3.1 ± 3.6	14.2 ± 6.4	3.7	−1.7 ± 0.6	2	3.9	2.2	Low intensity after decline
			TB	0.5 ± 0.3	9.4 ± 4.5	3.2	5.0 ± 1.8	2	8.1	2.0	
			BB	0.03 ± 0.02	5.2 ± 4.8	2.6	1.6 ± 0.3	2	12.6	1.7	
Observation V:											
V-1	1977 Sep 20	18:20	PL	53.8 ± 3.9	7.1 ± 0.2	2.9	−1.9 ± 0.04	2	344	34.0	Steady intensity
			TB	7.7 ± 0.3	3.4 ± 0.1	2.2	4.3 ± 0.1	2	68.3	33.0	
			BB	0.51 ± 0.02	0.0 ± 0.1	0.0	1.5 ± 0.02	2	56.3	31.4	
V-2	21	10:37	PL	45.5 ± 3.8	7.7 ± 0.2	3.0	−1.9 ± 0.05	2	177	29.8	Steady intensity
			TB	6.6 ± 0.3	4.0 ± 0.2	2.3	4.4 ± 0.1	2	28.3	29.0	
			BB	0.36 ± 0.02	0.0 ± 0.1	0.0	1.58 ± 0.02	2	33.0	28.1	
V-3	21	13:15	PL	311 ± 25	9.1 ± 0.2	3.2	−2.7 ± 0.05	2	174	42.4	1[h] before transition
			TB	23.1 ± 0.9	4.3 ± 0.1	2.4	2.7 ± 0.05	2	9.6	41.6	
			BB	1.7 ± 0.08	0.4 ± 0.1	1.0	1.22 ± 0.01	2	24.3	41.7	
V-4	21	14:14	PL	1473 ± 119	9.4 ± 0.2	3.2	−3.5 ± 0.05	2	76.2	62.6	Peak before transition
			TB	70.4 ± 3.0	4.1 ± 0.1	2.3	1.89 ± 0.03	2	5.8	62.3	
			BB	6.2 ± 0.3	0.5 ± 0.1	1.0	0.99 ± 0.01	2	25.9	64.0	
V-5	21	14:45	PL	31 ± 19	6.1 ± 1.1	2.7	−2.8 ± 0.4	2	4.5	5.2	30[m] after transition
			TB	2.7 ± 0.8	2.0 ± 0.6	1.8	2.4 ± 0.4	2	2.2	5.2	
			BB	0.5 ± 0.3	0.0 ± 0.8	0.0	1.0 ± 0.1	2	11.9	4.9	
V-6	21	16:19	PL	6.0 ± 5.2	3.2 ± 1.5	2.1	−2.3 ± 0.5	2	0.1	3.1	2[h] after transition
			TB	0.9 ± 0.4	0.2 ± 0.8	0.8	3.0 ± 0.8	2	0.6	3.3	
			BB	0.5 ± 0.7	0.0 ± 2.1	0.0	0.8 ± 0.2	2	16.8	2.7	

TABLE 2—*Continued.*

Spectrum No.	Date	Time (UT)	Spectrum Type[a]	I_0 (cts cm^{-2} s^{-1} keV^{-1})	N_H[b] (10^{22} atoms cm^{-2})	E_a[c] (keV)	α or kT (keV)	DOF	χ^2	L_x (1–20 keV)[d] (10^{37} ergs s^{-1})	Comments
V-7	22	06:17	PL	342 ± 258	8.1 ± 1.4	3.0	−4.1 ± 0.5	2	11.3	8.3	Soft flare
			TB	13.0 ± 5.1	2.7 ± 0.7	2.0	1.5 ± 0.2	2	11.1	8.5	16[h] after
			BB	1.8 ± 0.9	0.0 ± 0.8	0.0	0.8 ± 0.1	2	12.6	9.0	transition
V-8	22	09:37	PL	252 ± 94	9.3 ± 0.8	3.2	−3.5 ± 0.2	2	2.0	10.7	
			TB	13.7 ± 2.7	4.3 ± 0.4	2.4	1.8 ± 0.1	2	8.0	10.5	
			BB	1.3 ± 0.3	0.8 ± 0.4	1.2	0.95 ± 0.04	2	10.9	10.7	
V-9	22	10:44	PL	32 ± 19	8.1 ± 1.3	3.0	−2.7 ± 0.4	2	0.1	4.7	
			TB	2.8 ± 0.9	3.8 ± 0.8	2.3	2.5 ± 0.4	2	1.9	4.5	
			BB	0.25 ± 0.09	0.3 ± 0.7	0.9	1.1 ± 0.1	2	3.9	4.5	
V-10.....	22	19:04	PL	12.0 ± 4.8	12.2 ± 1.8	3.5	−1.9 ± 0.2	2	79.8	5.8	
			TB	1.5 ± 0.3	7.7 ± 1.3	3.0	4.4 ± 0.5	2	42.6	5.6	
			BB	0.06 ± 0.01	2.0 ± 1.0	1.8	1.7 ± 0.1	2	12.3	5.5	
V-11.....	23	12:20	PL	17 ± 18	51 ± 12	6.0	−1.9 ± 0.4	2	129	5.2	
			TB	0.18 ± 0.03	2.1 ± 1.1	1.8	36 ± 18	2	81.1	5.3	
			BB	0.005 ± 0.001	0.0 ± 1.6	0.0	3.0 ± 0.2	2	54.8	5.2	
V-12.....	23	17:06	PL	149 ± 61	42.4 ± 3.8	5.6	−2.4 ± 0.2	2	229	14.5	Hard spectrum
			TB	2.9 ± 0.4	17.7 ± 1.8	4.1	6.0 ± 0.5	2	149	14.4	intensity increase
			BB	0.046 ± 0.004	3.4 ± 0.8	2.2	2.3 ± 0.05	2	16.8	14.2	
V-13.....	24	01:32	PL	13.9 ± 3.1	15.0 ± 1.4	3.8	−1.5 ± 0.1	2	117	14.5	2[d]5 after transition
			TB	2.1 ± 0.2	9.4 ± 0.9	3.2	6.5 ± 0.4	2	38.5	14.1	
			BB	0.061 ± 0.006	2.2 ± 0.6	1.9	2.1 ± 0.05	2	1.2	13.5	
V-14.....	24	20:22	PL	13.3 ± 5.0	28.6 ± 3.5	4.9	−1.5 ± 0.2	2	82.0	12.9	
			TB	1.3 ± 0.2	14.8 ± 1.9	3.8	9.7 ± 1.1	2	48.2	12.9	
			BB	0.020 ± 0.002	2.2 ± 1.0	1.9	2.7 ± 0.1	2	9.3	12.4	
V-15.....	25	05:51	PL	23 ± 13	49.8 ± 6.7	6.0	−1.7 ± 0.2	2	107	10.2	
			TB	1.6 ± 0.3	32.7 ± 4.5	5.1	7.8 ± 1.2	2	100	10.1	
			BB	0.008 ± 0.001	1.2 ± 1.3	1.5	3.2 ± 0.1	2	46.7	10.4	
V-16.....	25	13:09	PL	37 ± 20	60.9 ± 7.2	6.4	−1.8 ± 0.2	2	102	11.3	
			TB	2.1 ± 0.4	42.3 ± 5.0	5.6	7.2 ± 0.9	2	99.3	11.2	
			BB	0.019 ± 0.004	17.3 ± 4.0	4.0	2.7 ± 0.1	2	93.3	10.9	
Observation VI:											
VI-1	1977 Oct 6	16:59	PL	0.05 ± 0.02	1.0 ± 2.0	1.4	+0.3 ± 0.2	2	8.8	4.8	Before intensity
			TB								increase
			BB	0.0006 ± 0.0002	0.0 ± 4.8	0.0	5.6 ± 0.8	2	40.0	4.9	
VI-2	7	04:04	PL	1.7 ± 1.1	30.5 ± 7.8	5.0	−0.8 ± 0.3	2	2.6	7.8	
			TB	0.5 ± 0.1	22.6 ± 5.4	4.4	18 ± 6	2	0.9	7.9	
			BB	0.004 ± 0.001	4.5 ± 3.7	2.4	3.6 ± 0.3	2	3.1	7.7	
VI-3	7	10:50	PL	3.1 ± 1.3	24.9 ± 4.5	4.6	−0.9 ± 0.2	2	8.9	12.2	
			TB	0.8 ± 0.1	17.3 ± 2.9	4.0	15.8 ± 3.1	2	2.8	12.3	
			BB	0.009 ± 0.002	3.5 ± 1.9	2.2	3.2 ± 0.1	2	14.3	11.8	
VI-4	7	20:41	PL	4.4 ± 1.9	23.7 ± 4.3	4.5	−1.1 ± 0.2	2	25.4	10.3	Peak before
			TB	0.8 ± 0.1	14.4 ± 2.6	3.8	12.3 ± 2.1	2	9.9	10.3	transition
			BB	0.011 ± 0.002	2.3 ± 1.4	1.9	2.9 ± 0.1	2	6.3	9.9	
VI-5	7	22:52	PL	1.0 ± 1.0	42 ± 14	5.6	−0.9 ± 0.4	2	19.1	3.9	After transition
			TB	0.24 ± 0.09	31 ± 10	5.0	18.1 ± 9	2	19.6	3.9	
			BB	0.0011 ± 0.0004	0.0 ± 3.2	0.0	4.3 ± 0.5	2	18.0	4.0	
VI-6	8	07:07	PL	0.3 ± 0.2	4.0 ± 2.1	2.3	−0.6 ± 0.2	2	0.3	3.5	
			TB	0.16 ± 0.04	2.5 ± 1.5	2.0	19.4 ± 9.2	2	0.3	3.5	
			BB	0.006 ± 0.002	0.0 ± 2.0	0.0	2.5 ± 0.3	2	19.9	2.9	

TABLE 2—*Continued.*

Spectrum No.	Date	Time (UT)	Spectrum Type[a]	I_0 (cts cm^{-2} s^{-1} keV^{-1})	N_H[b] (10^{22} atoms cm^{-2})	E_a[c] (keV)	α or kT (keV)	DOF	χ^2	L_x (1–20 keV)[d] (10^{37} ergs s^{-1})	Comments
Observation VIII:											
VIII-1 ...	1978 Aug 16	02:57	PL	1.0 ± 1.1	6.0 ± 3.2	2.7	−1.4 ± 0.6	1	4.1	1.7	Before
			TB	0.2 ± 0.1	3.3 ± 2.2	2.2	5.7 ± 2.7	1	2.0	1.6	intensity increase
			BB	0.01 ± 0.01	0.0 ± 2.1	0.0	1.7 ± 0.3	1	0.9	1.5	
VIII-2 ...	16	10:47	PL	3041 ± 5510	43 ± 12	5.7	−4.4 ± 0.8	1	0.2	6.0	
			TB	23 ± 18	27.4 ± 7.5	4.8	1.9 ± 0.4	1	4.2	5.8	
			BB	1.5 ± 1.5	22.6 ± 8.8	4.4	1.0 ± 0.1	1	7.9	5.6	
VIII-3 ...	16	12:20	PL	20 ± 29	17.3 ± 6.4	4.0	−2.6 ± 0.7	1	0.7	2.1	
			TB	1.4 ± 1.0	11.2 ± 4.6	3.4	2.9 ± 0.9	1	0.0004	2.0	
			BB	0.08 ± 0.07	6.3 ± 4.3	2.8	1.3 ± 0.2	1	0.37	1.9	
VIII-4 ...	17	08:39	PL	97 ± 81	25.1 ± 4.9	4.6	−2.8 ± 0.4	1	24.7	5.4	
			TB	3.9 ± 1.4	15.6 ± 3.0	3.9	3.0 ± 0.4	1	7.7	5.1	
			BB	0.17 ± 0.06	8.7 ± 2.4	3.1	1.4 ± 0.1	1	1.0	5.0	
VIII-5 ...	17	13:20	PL	57 ± 17	11.6 ± 0.9	3.5	−2.5 ± 0.2	1	2.4	10.4	
			TB	5.2 ± 0.8	6.8 ± 0.6	2.8	3.0 ± 0.2	1	1.2	9.8	
			BB	0.36 ± 0.06	2.7 ± 0.6	2.0	1.3 ± 0.05	1	8.8	9.3	
VIII-6 ...	18	01:49	PL	27 ± 17	15.4 ± 2.7	3.8	−2.4 ± 0.3	1	6.6	4.4	
			TB	2.2 ± 0.7	9.8 ± 1.9	3.3	3.2 ± 0.5	1	0.6	4.2	
			BB	0.12 ± 0.04	4.8 ± 1.7	2.5	1.4 ± 0.1	1	0.5	4.0	
VIII-7 ...	18	23:42	PL	95 ± 100	28.3 ± 7.0	4.8	−2.9 ± 0.5	1	24.4	4.7	Before
			TB	2.7 ± 1.0	15.4 ± 3.4	3.8	3.3 ± 0.5	1	7.3	4.6	intensity decline
			BB	0.1 ± 0.03	7.5 ± 2.5	2.9	1.5 ± 0.1	1	0.2	4.5	
VIII-8 ...	19	02:44	PL	2.2 ± 2.7	10.3 ± 4.9	3.3	−1.7 ± 0.6	1	9.7	1.6	At end of
			TB	0.3 ± 0.2	6.5 ± 3.5	2.8	4.8 ± 1.9	1	5.5	1.5	intensity decline
			BB	0.014 ± 0.009	1.2 ± 2.8	1.5	1.7 ± 0.3	1	1.5	1.5	
VIII-9 ...	19	13:45	PL	1.6 ± 4.6	6.5 ± 6.9	2.8	−2.0 ± 1.7	1	0.2	0.9	
			TB	0.2 ± 0.3	3.0 ± 4.2	2.1	3.9 ± 3.8	1	0.1	0.8	
			BB	0.02 ± 0.04	0.0 ± 4.2	0.0	1.4 ± 0.6	1	0.1	0.8	

[a] PL: $dF/dE = I_0 \exp[-\sigma(E)N_H]E^{\alpha}$ keV cm^{-2} s^{-1} keV^{-1}. TB: $dF/dE = I_0 \exp[-\sigma(E)N_H]e^{-E/kT}$ keV cm^{-2} s^{-1} keV^{-1}. BB: $dF/dE = I_0 \exp[-\sigma(E)N_H]E^3(e^{E/kT}-1)^{-1}$ keV cm^{-2} s^{-1} keV^{-1}. The quantify $\sigma(E)$ is the cross section for interstellar absorption (Brown and Gould 1970).

[b] When $N_H < 0$, it was fixed at 0.0 and other parameters determined.

[c] $\sigma(E)N_H \approx (E_a/E)^{8/3}$.

[d] For $d = 10$ kpc.

[e] The parameters were obtained from a least-squares fit to data from 3–5 energy channels. The errors represent the extent of the 1 σ error contour for a parabolic minimum.

the observation after transition, except when the detectors drifted off the source.

b) Observation II (Figs. 1*a*, 3)

Spectra II-1 and II-2 (Table 2) suggest that the flux increase at the beginning of Observation II (Fig. 1*a*) was due primarily to a decrease in absorption. Less absorption (II-2) is indicated by relatively large increases in low energy (<6 keV) flux. The flux changes in the four orbits preceding the transition are also related to changes in absorption parameters (II-3 to II-6). However, the transition itself (II-6 to II-7) is characterized by large decreases in the intensity parameters, spectral hardening, and a further decrease in absorption parameters.

The Observation II transition occurred during an orbit of mode B ($\frac{1}{8}$ ms) data, so limited intensity information and no spectral information are available for 2 hours around the transition time. Plots of intensities and spectral ratios for the preceding and following orbits are presented in Figure 3. The general characteristics are similar to the orbits surrounding the transition in Observation I (Fig. 2). No large intensity dip was seen in Observation II, but several small dips and flares lasting ~ 1 minute are apparent at energies <6 keV. The mode B data during the transition orbit showed a factor of 2 intensity decrease in ≤ 5 minutes during a tape recorder playback (20:27–20:32 UT) and another factor of 2 decrease occurred during Earth occultation (20:40–21:10 UT). Other than these changes, no abrupt drop in source intensity, which would mark the transition, was observed.

c) Observation III (Fig. 1*b*)

At the beginning of Observation III the source intensity was low and the spectrum (III-1 in Table 2) was relatively hard ($\alpha = -1.0$). About 17 hours before the transition, the intensity increased and the spectrum softened. From that time through the transition, the α and kT spectral parameters stayed nearly constant (spectra III-2 to III-7). The large intensity dip lasting ~ 4 hours near 1977 January 15.6 is correlated primarily with changes in the absorption parameters (III-3 to III-6). In addition, many large rapid intensity fluctuations (brief flares and dips by factors of 2–3 lasting 30–100 s) were evident during the mode B data and the brief segments of mode A data for the few orbits prior to transition. (This was primarily a mode B observation; see Table 1.) The Observation III transition (factor of 4 decrease occurred during the 30 minute Earth occultation in an orbit of mode B (1 ms) data. Lacking the high-statistics mode A data, we could not follow the detailed evolution of the source intensity or spectrum through the transition. However, spectral fits before and after the transition (III-6 and III-7) indicate only a modest change in absorption parameters.

d) Observation IV (Fig. 1*c*)

As suggested above, the early and gradual intensity decline in Observation IV is probably not a normal transition event. The spectra at maximum intensity (IV-2) and during the intensity decline (IV-3) are quite steep ($\alpha = -4$) and are highly cut off ($N_H \sim 2 \times 10^{23}$ atoms cm^{-2} for power law spectra); note the low counting rates in the 1.2–3 keV channel. Before the intensity increase (IV-1) and after the decline (IV-4) the spectra are harder ($\alpha = -2$) with much lower absorption parameters. Intensity fluctuations by factors of $\lesssim 2$ lasting 10–40 s are evident in the mode A data segments, particularly during the relatively high intensity period (May 9.5–10.4).

e) Observation V (Figs. 1*d*, 4*a*, 4*b*, 5)

During Observation V, Cir X-1 was brightest and displayed the greatest variety in its behavior. The uncorrected counting rates in four energy channels with 16.6 s resolution for the 1977 September 21 transition are displayed in Figure 4*a*. An expanded view of the transition with counting rate ratios is presented in Figure 4*b*. The 12:42 UT pretransition intensity dip and corresponding counting rate ratios are expanded in Figure 5. The background rates in Figure 4*a* are those measured during the Earth occultations. For the time shown in Figure 4*a*, the detectors were pointed continuously $\sim 0.^{\circ}2 \pm 0.^{\circ}1$ from Cir X-1. The total variation in counting rate due to satellite motion and background variation is at most $\sim 8\%$ of the counting rates displayed. Such variations would occur slowly over several minutes. Several types of intensity behavior apparent in Figure 4*a* are discussed below: (1) an unusual (for Cir X-1) steady state; (2) large intensity dips while the source brightens, softens, and becomes more chaotic; (3) a very rapid transition from high to low intensity; (4) large flares immediately after the transition; and (5) substantial X-ray flux after the factor of 10 intensity decrease during the transition.

Cir X-1 was in an unusually steady intensity state during the first 19 hours of Observation V. The final ~ 90 minutes of this steady state are shown in Figure 4*a*. The intensity of Cir X-1 did not vary by more than 20%, and the ratios of counting rates in the 1.2–3, 3–6, and 6–12 keV channels remained constant within statistical uncertainties. Spectral parameters determined near the beginning and end of this interval are essentially identical (V-1 and V-2 in Table 2), although the large χ^2 values indicate that the standard spectral forms do not adequately describe the data. Fourier analyses of data taken during this interval with 0.4 s and 1 ms resolution indicate that no periodic pulsations with periods 2 ms–1000 s were present (99.9% confidence) with more than 3% of the power from the source (see § IV). Autocorrelation analysis of the 1 ms data (see § V and Fig. 7*c*) indicate that the usual ~ 0.5 s aperiodic component of Cir X-1 was absent.

Large dips occurred in the Cir X-1 intensity from September 21 12:30 UT (Figs. 4*a*, 5) up to the transition. In direct contrast to the large dip before the Observation I transition (Fig. 2), the 1977 September 21 12:42 UT dip (Fig. 5) exhibits little change other than an indication of a 25% softening in the 3–6 keV/1.2–3 keV ratio. The rapid dip preceding this by 5 minutes may exhibit a trace of hardening, however. Other large intensity dips lasting

3–300 s during the 2 hours preceding the Observation V transition (Fig. 4*a*) show little or no change in the spectral ratios.

Although spectral changes are not notable during individual intensity dips, the Cir X-1 spectrum steadily softens during the period of chaotic intensity variation and rise to peak brightness in the two hours before the Observation V transition. This spectral evolution is apparent in the counting rates (Fig. 4*a*) and the counting rate ratios (compare Figs. 5 and 4*b*.). Large increases occur in both the 1.2–3 keV and 3–6 keV channels while the peak rates of the three orbits in the 6–12 keV channel remain nearly the same and the 8–19 keV flare diminishes. The softening is indicated quantitatively in the spectral parameter fits (V-2 to V-4 in Table 2). The thermal bremsstrahlung temperature decreases from 4.4 keV to 2.7 keV to 1.9 keV with essentially no change in absorption.

The 1977 September 21 transition was quite abrupt. The 1–20 keV luminosity decreased by a factor of 5 from a peak of 6×10^{38} ergs s^{-1} ($d = 10$ kpc) in 1 minute and decreased by another factor of 2 in 10 minutes. The parameters derived from spectral fits before (V-4) and after (V-5) the transition show a hardening of the spectrum (thermal bremsstrahlung temperature from 1.9 keV to 2.4 keV) and a decrease in the absorption parameter.

The bright flares after the Observation V transition each lasted 3–20 s and had a peak 1–20 keV luminosity of $1\text{–}5 \times 10^{38}$ ergs s^{-1}. The integrated luminosity of the largest flare is $\sim 1 \times 10^{40}$ ergs. As seen from the counting rate ratio plots in Figure 4*b*, the flares showed no pronounced spectral dependence, although a slight ($< 30\%$) hardening (3–6 keV/1.2–3 keV) can be discerned for the brighter flares. The flares of Observation V, with their abrupt rises and falls and lack of spectral variability, seem to be closely related to the chaotic intensity changes that preceded the transition.

The X-ray luminosity of Cir X-1 $\frac{1}{2}$ hour after the Observation V transition was 5×10^{37} ergs s^{-1} (1–20 keV) compared with 6×10^{38} ergs s^{-1} just before the transition (V-4 and V-5 in Table 2). The luminosity gradually decreased over the next several hours (3×10^{37} ergs s^{-1} at 2 hours after transition) with a slight hardening of the spectrum and further decrease in the absorption parameter (V-6).

The evolution of the Cir X-1 flux and spectrum after the Observation V transition is presented in Figure 1*d*. A large flux increase (< 6 keV) occurred ~ 14 hours after the transition, at September 22.2. The flux increase lasted ~ 14 hours and hardened considerably as the flare progressed toward its conclusion (V-7 to V-10). About 14 hours later another intensity increase occurred with an even harder spectrum and large flux in the 8–19 keV channel (V-11 to V-16). The spectrum remained hard at least until Cir X-1 approached detection threshold on September 26, 4.5 days after transition, just before the observation ended. Several intensity dips and flares (changes by factors of 2–3 for 20–120 s) occurred sporadically during the 4.5 days after the transition.

f) *Observation VI* (Figs. 1*e*, 6)

The X-ray spectrum was exceptionally hard ($\alpha = +0.3$; VI-1) when Cir X-1 reappeared October 6.6 (~ 1 day after the beginning of Observation VI) and remained hard ($\alpha \sim -1$; VI-2 to VI-6) during the observation (Fig. 1*e*). The spectrum was highly cut off with very little flux in the 1.2–3 keV channel throughout Observation VI. Comparison of spectral parameters before and after transition (VI-4 and VI-5) suggest a hardening of the spectrum and an increase in the column density parameter, in contrast to the other observations.

A more detailed view of the orbits around the Observation VI transition time is presented in Figure 6. Large (factor 2–4) intensity dips lasting 20–150 s are evident in the orbits preceding transition. The transition (factor of 3 decrease in the 3–6 keV channel) apparently occurred during Earth occultation ($\sim$22:30 UT). This was followed by the brief brightening episode seen at $\sim$23:30 in Figure 6. About 7 hours after transition, several short (20–60 s) flares (increases by factors of 2–3) occurred in one orbit of data. These flares preceded the brightening of Cir X-1 (October 8.3; Fig. 1*e*) before it faded below detection threshold.

g) *Observation VII* (Fig. 1*f*)

During Observation VII, Cir X-1 was above detection threshold only in the 3–6 keV channel (Fig. 1*f*). In spite of this low intensity, there is a definite change in intensity level from before June 13.1 to after June 13.5. During most of this interval, Cir X-1 was near the edge of our detector field of view so that counting rate uncertainties are highly magnified when counting rates are corrected for pointing offset.

h) *Observation VIII* (Fig. 1*g*)

The Cir X-1 spectrum was hard ($\alpha = -1.4$; VIII-1 in Table 2) at the beginning of the observation (Fig. 1*g*). Then after a brief soft flare ($\alpha = -4.4$; VIII-2), the source brightened and the spectrum retained a nearly constant shape ($\alpha = -2.6$; VIII-3 to VIII-7) with some changes occurring in the absorption parameter. As the transition occurred, the spectrum hardened again (to $\alpha = -1.7$; VIII-8) and the absorption parameter decreased. This intensity decrease amounted to a factor of 3 in 5 hours and preceded the expected transition time (August 19.7) by ~ 0.6 days. Observations VII and VIII were directed toward searches for millisecond bursts; hence only short segments of high statistics mode A data with spectral information are available.

IV. PULSE PERIOD UPPER LIMITS

Cir X-1 exhibits large intensity variations on many time scales, but periodic pulsations have not been detected. Rocket and satellite scans lasting a few tens of seconds have suggested the presence of brief pulse trains with periods of 0.7 s (Margon *et al.* 1971) 2.2 s (Toor 1977) and 2.5 s (Sadeh *et al.* 1979). However, these pulse trains are not persistent and may be simply manifestations of the aperiodic variability of the source. *Uhuru*

observations yielded no stable period in the range 0.2–20 s (Jones *et al.* 1974). A rocket flight with 1 ms resolution placed a 3 σ upper limit on stable pulsations with periods of 2 ms–10 s and amplitudes greater than 3% of the source intensity (Spada *et al.* 1974).

Pulse period upper limits derived from extensive Fourier analyses of our pointed observations of Cir X-1 are presented in Tables 3A and 3B. Long (up to 6 days) fast Fourier transforms (FFT) were performed on the mode A data of Observations II, V, and VI with 0.41 s and 0.83 s resolution. In each case, we approximated and fitted the observed power density as a function of frequency with the sum of a power law which dominates at low frequencies ($\lesssim$0.1 Hz) plus a constant term due to white noise from the counting statistics which dominates at higher frequencies ($\gtrsim$0.1 Hz), i.e., $P = C_1 \nu^{-\gamma} + C_2$. The distribution of power densities near a given frequency was assumed to be exponential. With this model to define the local mean at any frequency, we searched for values of power density significantly greater than the local mean. After dividing by the local mean, the overall distribution of power densities remained approximately exponential. Thus, we are able to estimate the 99.9% confidence level for a given excursion in any frequency bin. The corresponding pulse *amplitude* divided by the average counting rate is frequency dependent and has the form $[A\nu^{-\gamma} + B]^{1/2}$. The parameters A, B, and γ are given in Table 3A, together with percentage upper limits at sample periods.

The shortest period to which we are sensitive with the

TABLE 3A

PULSE PERIOD LIMITS ($P > 0.8$ s)[a]

OBSERVATION AND DATES	ENERGY (keV)	SOURCE (counts s^{-1})	LIMIT PARAMETERS A	γ	B	PERCENTAGE POWER UPPER LIMITS FOR SAMPLE PERIODS (%) 0.8–1.7 s[b]	1.7 s	30 s	5 min	30 min	3 hr
Obs. II,											
1976 Dec 10.4–13.7	1.2–12	24	1.3×10^{-7}	1.40	1.2×10^{-5}	0.29	0.35	0.52	2.0	6.9	24
	6–19	4.5	6.0×10^{-9}	1.76	1.6×10^{-4}		1.3	1.3	1.7	5.8	28
Obs. V,											
1976 Sep 20.7–21.6	1.2–12	130	8.0×10^{-9}	1.79	6.2×10^{-6}	0.25	0.25	0.31	1.5	7.3	36
	6–19	35	2.0×10^{-9}	2.04	2.9×10^{-5}		0.54	0.56	1.6	9.4	58
Obs. V,											
1977 Sep 22.9–26.3	1.2–12	18.0	3.5×10^{-8}	1.58	1.0×10^{-5}	0.36	0.32	0.42	1.7	7.0	29
	6–19	14.9	2.9×10^{-8}	1.55	1.5×10^{-5}		0.39	0.45	1.5	5.7	23
Obs. VI,											
1977 Oct 5.0–11.3	1.2–12	3.3	1.0×10^{-7}	1.71	9.5×10^{-5}	3.2	1.0	1.1	4.3	19	89
	6–19	4.8	9.9×10^{-8}	1.62	5.9×10^{-5}		0.77	0.91	3.3	14	58

[a] For periods $\gtrsim$1.7 s, the transformed time bins were of 0.83 s duration, and the upper limit (99.9% confidence of occurrence in any frequency bin) for the *fractional* power above the local mean in the PDS at a given frequency is approximated by $(A\nu^{-\gamma} + B)^{1/2}$, where A and B are constants and ν is given in Hz. For periods <1.7 s, limits were determined only from 1.2–6 keV data; data with time resolution of 0.41 s are available only in this range.

TABLE 3B

PULSE PERIOD LIMITS ($P < 4$ s)

Observation	Periods	Number of Transforms[a]	Source Counts	Background Counts	Percentage Pulsed Power Upper Limit (99.9%)
Obs. II	250 μs–0.5 s	954	7.7×10^4	1.0×10^4	4.7
	2 ms–1 s[b]	922	5.2×10^5	8.7×10^4	1.8
Obs. III	250 μs–0.5 s	8918	3.6×10^5	7.1×10^4	3.9
	2 ms–0.5 s	1441	2.6×10^5	7.9×10^4	3.0
Obs. IV	250 μs–0.5 s	13,640	4.8×10^5	1.1×10^5	3.8
	2 ms–0.5 s	2057	3.0×10^5	1.1×10^5	3.2
Obs. V[c]	2 ms–1 s	1691	9.1×10^5	9.3×10^4	1.6
Obs. VIII	250 μs–0.5 s	31,765	4.5×10^5	3.3×10^5	4.5
	2 ms–4 s	2010	1.8×10^5	1.8×10^5	4.9

[a] The individual transforms of duration 0.5 s (or 4 s) were added to obtain the indicated limits. In most cases, the data are the sum of the 1.2–12 keV rates from the horizontal-tube detector and the 1.6–15 keV rates from the center and right slat detectors.

[b] The higher limits at longer periods seen in Table 3A are also evident in the transforms of 1 ms data for periods of 0.5 s to 4 s for Obs. II, III, IV, and V. In each case the upper limit at 4 s is less than a factor of $\sim$2 above the given limit.

[c] The mode B data of Observation V is in four pieces of $\sim$2 hr each taken on 1977 Sep 21.2, 24.1, 25.1, 26.4.

mode A data is 0.83 s in the 1.2–6 keV range since the data sampling period for mode A in that range is 0.41 s. For data above 6 keV the sampling period is 0.83 s. Although the upper limits from the fits reach 100% at periods of several hours, the actual power spectra show some evidence of flattening out before that occurs, so that the indicated limits for periods of hours may be overestimates. The frequencies of the highest power components in the several data sets were compared in an attempt to discover peristent longer periods. No reoccurrences of the same frequency were found. Background rates were assumed constant at 10 counts s^{-1} for the 1.2–12 keV channel and 12 counts s^{-1} for the 6–19 keV channel. We find no significant pulsations during either the bright pretransition states of Cir X-1 or in the hard spectrum state following the 1977 September 21 transition.

All the 1 ms and $\frac{1}{8}$ ms mode B data have been searched for high frequency (periods < 4 s) pulsations. Each high-speed event monitor block of 4096 points was transformed with an FFT, and the resulting power densities were summed for each observation. The high frequency limits thus obtained are given in Table 3B. Aperiodic variability (See § V) with characteristic times of ~ 1 s often contributed larger than average values of power density for periods of 0.5–4.0 s. These larger values increase our pulse fraction upper limits in that range by a factor of ~ 2 over the corresponding limits for periods of < 0.5 s. We find no evidence that Cir X-1 exhibits regular pulsations.

V. APERIODIC VARIABILITY: 20 ms–1 s

Although not a pulsing source, Cir X-1 has long been known for its rapid irregular variations and similarity, in this respect, to Cyg X-1. *Uhuru* observed 2–6 keV variations by up to a factor of 3 in 0.1 s (Jones *et al.* 1974). The absence of significant autocorrelation for times from 0.4 s to 10 s in two days of 20 s *Uhuru* crossings of Cir X-1 indicates that the non-Poisson fluctuations observed in the data must occur on time

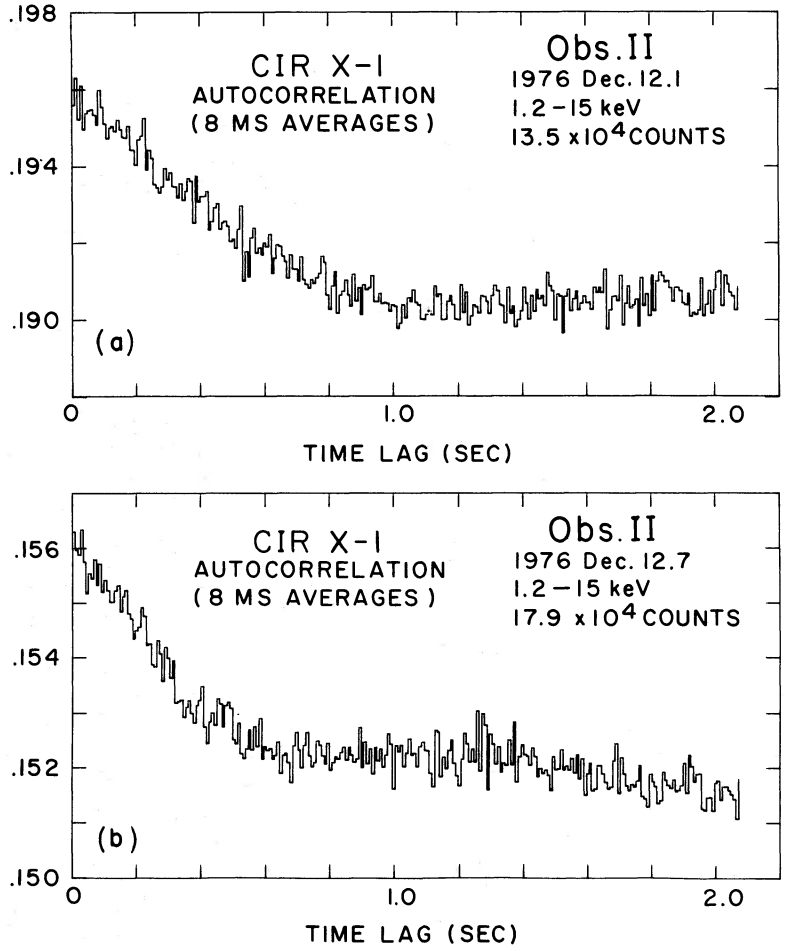

FIG. 7.—Autoccorelation functions for single orbits (~ 1200 s) of data. (*a*) Observation II, Dec 12.1, during maximum $\sim 20^h$ before transition (Fig. 2), (*b*) Observation II, Dec 12.7, during the slow pretransition dip (Fig. 2), (*c*) Observation V, Sep 21.2 steady intensity (Fig. 4*a*), (*d*) Observation V, Sep 24.1, during hard posttransition flaring (Fig. 1*d*). Note different decay times in Figs. 7*a* and 7*b* and the 20 ms component in Fig. 7*d*, seen only in this one orbit.

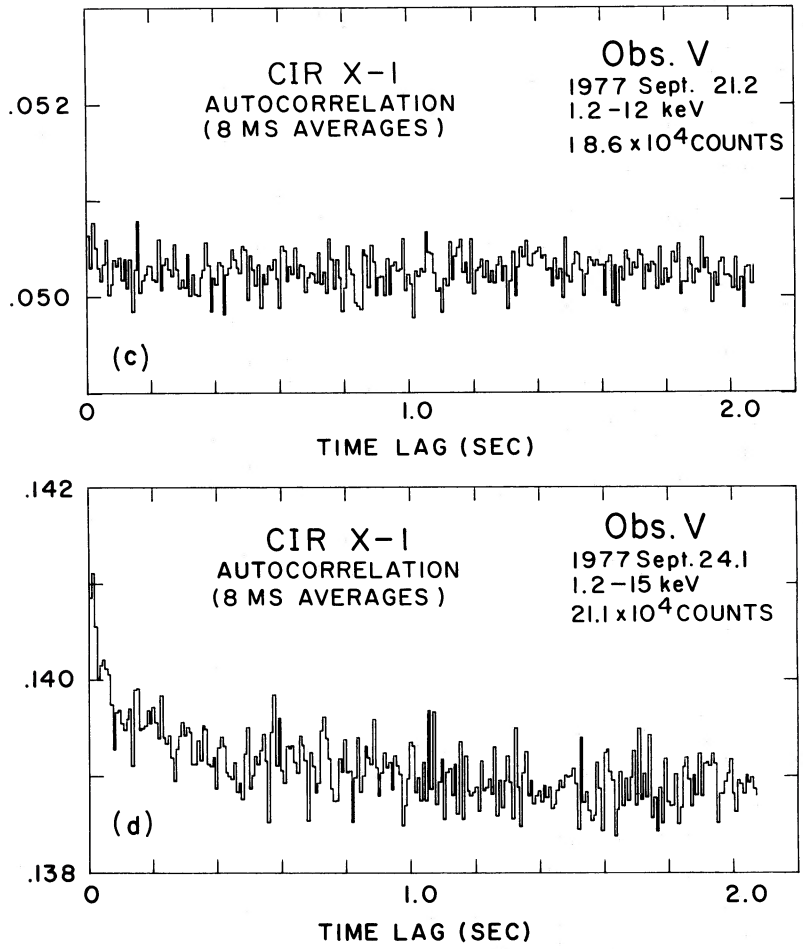

FIG. 7—*continued*

scales <0.4 s (Weisskopf and Sutherland 1980). However, autoccorelation analysis of 1 ms rocket data indicated the absence of aperiodic pulsations with characteristic times from 1 ms to 1 s containing more than 8% of the counts from Cir X-1 (Spada *et al.* 1974). Analysis of the present data indicates that aperiodic pulsations with characteristic times of 0.3–1.0 s are often, but not always, present in Cir X-1. Also, in contrast to Cyg X-1 (Sutherland, Weisskopf and Kahn 1978), the aperiodic variability of Cir X-1 is not readily modeled by simple shot noise plus a constant source.

Autocorrelation analyses were performed on the orbits of data with 1 ms resolution (Table 1). The autocorrelation functions (ACF) for four of these orbits (two from Observation II and two from Observation V) are presented in Figure 7*a*–7*d*. Each ACF is normalized to 1.0 at zero time delay, ACF(0) = 1.0. Since the mean is not subtracted from the data, the value of the ACF for large time lags indicates the average total counting rate (counts per ms). The linear decline of the Cir X-1 ACF in Figures 7*a* and 7*b* may be contrasted with the exponential decline (characteristic time of ~0.5 s) seen in the ACF of Cyg X-1 (Rothschild *et al.* 1977 and Fig. 8).

A linear decline in an ACF suggests, but does not require, a rectangular shape for aperiodic pulses. For a linear decline, we define the characteristic times as the time lag at which the straight line fit to the linear decline intersects the straight line fit to the ACF for large time lags. The characteristic time of the ACF in Figure 7*a* is 1.0 s, distinctly different from the 0.6 s characteristic time of Figure 7*b*. This suggests an evolution in the Cir X-1 system as it approached the transition of Observation II (1976 December 12.8). Data taken prior to the transition in Observation III and the decline of Observation IV yield ACFs similar to those of Figures 7*a* and 7*b* but with characteristic times of 0.3 s (Observation III) and 0.6 s (Observation IV).

Cir X-1 displayed erratic variability near the times represented in Figures 7*a* and 7*b*. Small flares lasting a few seconds and small intensity dips of similar duration were common. In contrast, the source intensity early in Observation V (1977 September 21.2) was unusually constant. As indicated previously, no periodic pulsations were found. The nearly flat ACF of Figure 7*c* indicates that no significant aperiodic pulsations were present at this time. A similar conclusion can be drawn from the

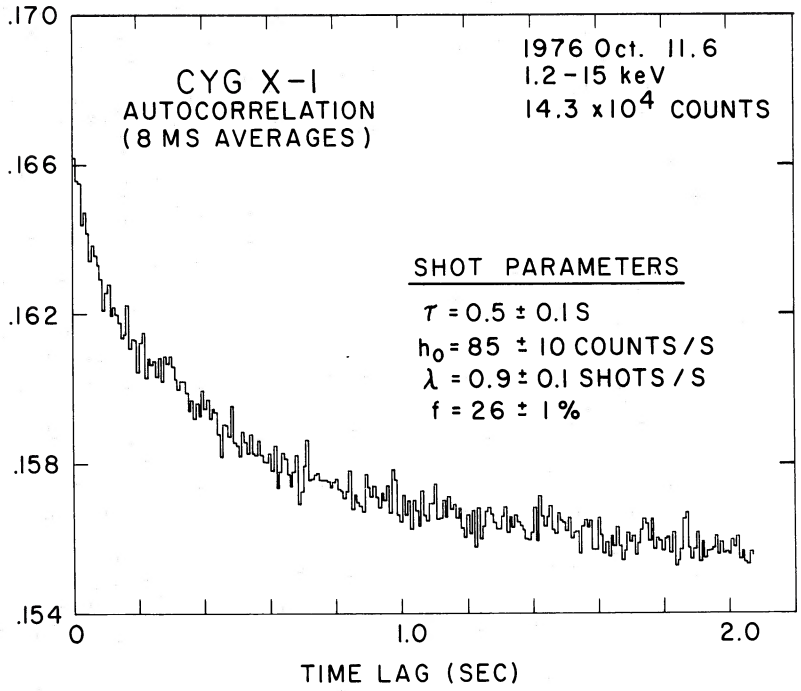

FIG. 8.—Cyg X-1 autocorrelation function and shot noise parameters

flat ACF plots derived from five orbits of 1 ms data obtained prior to the Observation VIII intensity decrease, including one orbit ~3 hours before the intensity decrease.

The data for Figures 7*a*–7*c* were taken within a day before the associated X-ray transitions when the source spectra were relatively soft (Table 2). In contrast, the data for Figure 7*d* were taken 2.5 days after the Observation V transition when the X-ray spectrum was relatively hard (Table 2; Fig. 1*d*). In this instance, the linear decline is much less pronounced, and there is a clear peak in the 1–24 ms bins indicating a ~20 ms component in the source variability. This is the only orbit of 1 ms data which contains this feature. A 20 ms component has also been noted in Cyg X-1 (Canizares and Oda 1977).

A simple shot noise model (Terrell 1972) for aperiodic variability is attractive because model parameters may be readily derived from the data. In the shot noise model, the aperiodic variability is attributed to a constant source plus a superposition of randomly occurring identical shot pulses characterized by an average shot rate (λ) and a fixed shape ($h[t, \tau]$) with a characteristic time (τ). The shape and characteristic time of the shots are suggested by the shape and characteristic time of the autocorrelation function. With these parameters fixed, the shot amplitude, shot rate, and shot fraction may be derived from the mean, variance, and third moment of the data. For exponential shots, the relations have been derived previously (Sutherland, Weisskopf, and Kahn 1978). For rectangular shots, we derived the following expressions for the case in which the data bin width, T, is less than the characteristic time of the shots τ:

mean: $\langle s \rangle = (\lambda h\tau + C)T$;

variance: $V_s = \lambda h^2 T^3(\tau/T - \frac{1}{3})$;

third moment: $M_{3s} = \lambda h^3 T^4(\tau/T - \frac{1}{2})$.

Then for $T \ll \tau$, we have

shot amplitude: $h_0 \approx \frac{M_{3s}}{V_s}\frac{1}{T}$;

shot rate: $\lambda \approx \frac{V_s^3}{M_{3s}^2}\frac{1}{\tau}$;

shot fraction: $f \equiv \frac{\lambda h\tau T}{\langle s \rangle} \approx \frac{V_s^2}{M_{3s}}\frac{1}{\langle s \rangle}$.

Here C is the constant source rate.

We find that a simple shot noise model does not account for the irregular variability of Cir X-1. Seven orbits of data with 1 ms resolution were analyzed for shot noise parameters. A linear decline in the autocorrelation function is clearly visible for each orbit of data. The orbits occurred before the transitions of Observations II, III, and IV (including the data for Figs. 7*a* and 7*b*) when source strength was greater than twice the background. The mean, variance, and third moment were computed for bin sizes of 16, 32, 64, 128, and 256 ms. In most cases, the third moment of the data was negative and close to zero, and the values of shot parameters varied greatly for different bin sizes.

Only one orbit of data (from 1976 December 12.4) produced consistent results for three different bin sizes. The ACF of those data is similar to that in Figure 7*a* with a characteristic time of 0.9 s. For rectangular shot pulses, we derived the following parameters:

$$h_0 = 7.6 \pm 0.5 \text{ counts s}^{-1} ;$$

$$\lambda = 16 \pm 2 \text{ shots s}^{-1} ;$$

$$f = 71 \pm 4\% .$$

The errors indicate the range of variation for different bin sizes. As a check, the formal procedure was applied to an orbit of data from Cyg X-1 taken with the same detectors. In that case, the mean, variance, and third moment computed for different bin sizes yielded the standard set of shot parameters which characterize Cyg X-1 (Weisskopf *et al.* 1978). Figure 8 displays the ACF and shot parameters derived from the data.

Simple shot noise may not be an appropriate physical model of X-ray source behavior (Doi 1978), and recent work indicates that simple time-asymmetric exponential shots may not be adequate for Cyg X-1 (Weisskopf *et al.* 1978). It is not surprising, then, that the simplest shot noise model fails to characterize the Cir X-1 data. However, the autoccorelation functions clearly show that the aperiodic X-ray emission from Cir X-1 often exhibits a $\sim$0.5 s feature and, in one case, a $\sim$20 ms feature.

VI. SEARCH FOR MILLISECOND BURSTS

The similarity of the rapid aperiodic variability in Cyg X-1 and Cir X-1 has prompted the search for millisecond bursts of X-rays from Cir X-1 similar to those reported from Cyg X-1 (Rothschild *et al.* 1974; Oda *et al.* 1974; Rothschild *et al.* 1977). A burst of X-rays from Cir X-1 lasting $\sim$10 ms with a peak rate of 16 times the average rate was detected in a rocket flight in 1976 (Toor 1977). Five smaller bursts were also reported from that observation of Cir X-1.

To search for similar bursts, we binned all our Cir X-1 data with $\frac{1}{8}$ ms resolution (Observations II, III, IV, VII, VIII; see Table 1) in 16 ms bins. For each orbit of data, the number of bins with a given number of counts was compared with the number of bins expected from Poisson statistics. The nonocculted orbit average was used as the mean counting rate. Individual 16 ms bins with excessive numbers of counts (probability of occurrence during the orbit <0.01) were then examined with $\frac{1}{8}$ ms resolution.

For Observations IV, VII, and VIII no millisecond bursts were detected in 4×10^4 s of $\frac{1}{8}$ ms resolution data. The data came from the combined outputs of the argon tube, center slat, and right slat detectors (230 cm^2 effective area total) over the energy range 1.2–15 keV. The duty cycle is 8% for the $\frac{1}{8}$ ms high-speed event monitor mode B data. (During Observations II and III, data from the failing left slat detector were included in the total. We believe the millisecond bursts reported after preliminary analysis [Dower, Bradt, and Canizares 1977] are spurious artifacts of the failing counter.)

Bright millisecond bursts of the type observed by Toor (1977) would have been detected in our observations. Our failure to see any indicates that such bursts must be extremely rare. Perhaps they are associated with the unusual spectral state noted by Toor in which the hardest spectra occurred at the highest (1–8 keV) count rates (Toor 1977).

VII. DISCUSSION

Cir X-1 is likely to be a compact object (e.g., neutron star or black hole) in a binary system with an OB supergiant star (Whelan *et al.* 1977) or, perhaps, a symbiotic star (Glass 1978). An adequate model of the details of the system must account for the wide variety of behavior observed at X-ray, optical, infrared, and radio energies: active and low intensity states that last for hundreds of days; the 16.6 day cycle with rapid X-ray intensity drop followed by sharp rises in optical, infrared, and radio fluxes; X-ray dips and flares over times of hours to seconds; aperiodic X-ray fluctuations with times of 1 s; and occasional millisecond X-ray bursts.

The long term active and low intensity states of the source may be related to changes in the mass loss rate of the companion star. The X-ray source 4U 0115+63 may provide an analogy for this long term behavior. Like Cir X-1, 4U 0115+63 has exhibited long intervals of low X-ray luminosity. It has an orbital period of $24\overset{d}{.}3$ (Rappaport *et al.* 1978) similar to the $16\overset{d}{.}6$ cycle of Cir X-1. The moderate eccentricity ($e = 0.34$) and relatively wide orbit of 4U 0115+63 may allow mass transfer sufficient to excite the X-ray source only during occasional episodes of large mass loss from the companion (Rappaport *et al.* 1978). This would account for the transient nature of 4U 0115+63. A similar explanation could be constructed for the long term behavior of Cir X-1.

Two types of flux modulation mechanisms may account for the $16\overset{d}{.}6$ cycle. A geometric modulation model assumes an intrinsically constant X-ray source which exhibits large apparent flux changes due to changes in the environment along the line of sight. An accretion modulation mechanism assumes that the varying X-ray source flux is due to changes in the accretion rate onto the compact object. Of course, combinations of the two mechanisms are also possible.

Purely geometric models do not seem adequate to explain the observations. For instance, following the X-ray transition the symmetric rise expected from a constant source undergoing a simple geometric eclipse is not observed. Also, a simple eclipse seems unable to explain the increases in optical, infrared, and radio fluxes that follow the X-ray decreases. These flux increases at longer wavelengths provide similar difficulties for a model of the X-ray transition based on screening of the X-ray source by a precessing accretion disk of the type proposed for the 35^d cycle of Her X-1 (Katz 1973; Merritt and Petterson 1980 and references therein). Also, increases in the column density of absorbing material suggested by the precessing disk model are not usually observed in the X-ray spectra at transition.

Models of Cir X-1 emphasizing a companion with a strong stellar wind have been proposed (Coe, Engel, and

Quenby 1976) and developed in some detail (Haynes *et al.* 1979; Fransson and Fabian 1980; Murdin *et al.* 1980). These detailed models suggest that the X-ray transition results when a constant spectrum source experiences increased absorption in the dense stellar wind near periastron in a highly elliptical orbit (Murdin *et al.* 1980) or in an X-ray induced shock front in the stellar wind (Fransson and Fabian 1980). Although we observed possible absorption events in Cir X-1 (Figs. 2, 1*a*, 1*b*; Table 2) before the transitions in Observations I, II, and III, the spectral fits in Table 2 and counting rates and ratios in Figures 1–6 indicate that the X-ray transitions are not due to a simple increase in the low energy cutoff produced by increased absorption for a one component source. Models based on changing absorption of a constant source also have difficulty explaining the rapidity (<2 minutes) of the transitions of Observations I and V (Figs. 2 and 4) and the extremely hard spectrum of the source throughout Observation VI (Fig. 1*e*).

A simple accretion modulation model in which the X-ray transition is due to reduced accretion flow at apastron of an eccentric orbit (Clark, Parkinson, and Caswell 1975) would seem to suggest a much more gradual decrease in X-ray flux than is observed (as little as 1–2 min.). Simply starving the X-ray source seems unable to produce the observed flux increases at longer wavelengths subsequent to transition.

The observed fast (<2 minutes) X-ray transitions of Observations I and V and the rapid dips and flares (e.g., Fig. 4) are suggestive of instabilities in accretion flow. Accretion modulation mechanisms for a rotating, magnetic neutron star have been developed (Baan 1977; Lamb *et al.* 1977) to account for the rapid (Type II) bursts of MXB 1730−335 (Lewin *et al.* 1976*a*; Hoffman, Marshall, and Lewin 1978) and for Type I bursts. The Cir X-1 flares following the Observation V transition are similar in shape, duration, intensity, and lack of spectral variability to the Type II bursts. The magnetic instabilities, if they are responsible for Type II bursts. would preclude steady accretion and steady X-ray emission, at least from the local region at which the bursts occur. In Cir X-1, there is a substantial steady component underlying the flares. Since the spectra of the steady and the flare components are nearly identical (see count ratios in Fig. 4), they appear to arise from the same region. Furthermore, two large flares from Cir X-1 (14:20:40 UT and 14:23:00 UT in Fig. 4) are immediately followed by other flares rather than the quiescent periods observed for large Type II bursts from MXB 1730−335. These points indicate different physical mechanisms or conditions for the Cir X-1 flares and the rapid (Type II) bursts.

The asymmetric light curves of the X-ray, optical, infrared, and radio fluxes around the time of the X-ray transition clearly indicate rapid physical changes which would occur near periastron in an eccentric orbit (Murdin *et al.* 1980). The dramatic 3 hour increase in the IR flux shortly after transition (Glass 1978) is a clear manifestation of this. The subsequent 10^{d} decay with no change in colors over the *J*, *M*, *K*, and *L* bands can be explained by the cooling of a very hot ($\gg 10^4$ K) or nonthermal source (Glass 1978). The separate radio peaks after X-ray transition are indicative of multiple explosive events. The radio observations (Haynes *et al.* 1978) are consistent (Haynes, Lerche, and Murdin 1980) with the van der Laan (1966) model of an adiabatically expanding synchrotron plasma that has been used to account for the radio outbursts of Cyg X-3 (Gregory and Seaquist 1974).

The rapidity (1 minute) of the Observation V transition and the lack of increase in absorption parameter for most of the transitions we observed suggest to us that the X-ray transition results from a disruption of the accretion process (Haynes, Lerche, and Murdin 1980) rather than X-ray absorption in the primary star's stellar wind (Murdin *et al.* 1980) or in shocks forming around the X-ray source (Fransson and Fabian 1980). A scenario which might account for the qualitative features of the Cir X-1 light curves at various energies is the following. Accretion flow into the compact object increases with the approach of periastron passage in an eccentric orbit (Clark, Parkinson, and Caswell 1975). This increases the X-ray flux which, in turn, increases the accretion flow via X-ray heating of the companion (Basko and Sunyaev 1973). This positive feedback process is halted by a disruption of the accretion process, perhaps related to a thermal instability (Cowie, Ostriker, and Stark 1978) or possibly to high radiation pressures at high accretion rates (e.g., 6×10^{38} ergs s^{-1} in Table 2; V-4). This might produce an expanding shell or shells of very hot ionized material which heats gas and dust surrounding the system to produce the infrared flux peak and interacts with the surrounding magnetic field to produce synchrotron peaks in the radio flux. A large quantity of expelled ionized matter which has cooled and recombined with electrons could produce the increased absorption of low energy X-rays (<3 keV) relative to the hard flux noted $2^{d}.5$ after the Observation V transition and through Observation VI. The sustained X-ray fluxes following the transitions indicate that accretion can continue after the disruptive event, but at a reduced level.

At the least, the similarities in the intensity changes, durations, and lack of spectral variability of the dips, transition, and flares of Observation V on 1977 September 21 (Figs. 4, 5) argue that a single modulating mechanism is responsible for these rapid phenomena and place significant constraints on models of Cir X-1. The notable similarities to and differences from the X-ray behavior of Cyg X-1 (Oda 1977) should also be helpful in restricting models. Cyg X-1, like Cir X-1, exhibits 0.5 s and 20 ms aperiodic variability (Brinkman *et al.* 1974; Weisskopf *et al.* 1978; Canizares and Oda 1977). Millisecond bursts may also occur in both sources (Rothschild *et al.* 1977; Toor 1977). Cyg X-1 also exhibits 2–6 keV X-ray flux decreases followed within ~ 1 week by radio flux increases (Tananbaum *et al.* 1972; Braes and Miley 1976). However, the 2–6 keV flux decrease is accompanied in Cyg X-1 by a 10–20 keV flux increase (Tananbaum *et al.* 1972). X-ray absorption dips lasting

a few hours or less have been observed in Cyg X-1 (Li and Clark 1974; Mason *et al.* 1974; Parsignault *et al.* 1976). However, Cyg X-1 does not exhibit the wide range of temporal and spectral variability seen in Cir X-1.

Much work remains to be done. Detection and studies of optical absorption lines could confirm that the $16^{d}.6$ cycle is an orbital period. Studies of the evolution of structure in the Hα line (reported by M. W. Feast in Glass 1978) are needed for evidence of expanding shells of material that might be expected from explosive models or shock front models (Haynes, Lerche, and Murdin 1980; Fransson and Fabian 1980). Finally, coordinated observations at several wavelengths during several $16^{d}.6$ transition episodes could elucidate more precisely the relationship between the X-ray, optical, infrared, and radio variability and further restrict possible mechanisms responsible for the behavior of this remarkable system.

We are pleased to thank the members of the Center for Space Research, in particular the *SAS 3* group, for their continued assistance. We are grateful to Claude Canizares and Paul Joss for helpful discussions, and to Trish Dobson and Steve Joyce for their assistance.

REFERENCES

Baan, W. 1977, *Ap. J.*, **214**, 245.
Baity, W. A., Ulmer, M. P., and Peterson, L. E. 1975, *Ap. J.*, **198**, 447.
Basko, M. M., and Sunyaev, R. A. 1973, *Ap. Space Sci.*, **23**, 117.
Bradt, H. V., Apparao, K. M. V., Dower, R., Doxsey, R. E., Jernigan, J. G., and Markert, T. H. 1977, *Nature*, **269**, 496.
Braes, L. L. E., and Miley, G. K. 1976, *Nature*, **264**, 731.
Brinkman, A. C., Parsignault, D. R., Schreier, E., Gursky, H., Kellogg, E. M., Tananbaum, H., and Giacconi, R. 1974, *Ap. J.*, **188**, 603.
Brown, R. L., and Gould, R. J. 1970, *Phys. Rev. D*, **1**, 2252.
Buff, J., *et al.* 1977, *Ap. J.*, **212**, 768.
Canizares, C. R., Li, F. K., and Clark, G. W. 1974, *Ap. J.* (*Letters*), **191**, L75.
Canizares, C. R., and Oda, M. 1977, *Ap. J.* (*Letters*), **214**, L119.
Clark, D. H., Parkinson, J. H., and Caswell, J. L. 1975, *Nature*, **254**, 674.
Coe, M. J., Engel, A. R., and Quenby, J. J. 1976, *Nature*, **262**, 563.
Cowie, L. L., Ostriker, J. P., and Stark, A. A. 1978, *Ap. J.*, **226**, 1041.
Davison, P. J. N., and Tuohy, I. R. 1975, *M.N.R.A.S.*, **173**, 33P.
Doi, K. 1978, *Nature*, **275**, 197.
Dower, R., Bradt., H., and Canizares, C. 1977, *Bull. AAS*, **9**, 297.
Forman, W., Jones, C., and Tananbaum, H. 1976, *Ap. J.*, **208**, 849.
Fransson, C., and Fabian, A. C. 1980, *Astr. Ap.*, **87**, 102.
Glass, I. S. 1976, *IAU Circ.*, No. 2974.
———. 1978, *M.N.R.A.S.*, **183**, 335.
———. 1979, *M.N.R.A.S.*, **187**, 807.
Goss, W. M., and Mebold, U. 1977, *M.N.R.A.S.*, **181**, 255.
Gregory, P. C., and Seaquist, E. R. 1974, *Ap. J.*, **194**, 715.
Gursky, H., *et al.* 1978, *Ap. J.*, **223**, 973.
Haynes, R. F., Jauncy, D. L., Murdin, P. G., Goss, W. M., Longmore, A. J., Simons, L. W. J., Milne, D. K., and Shellern, D. J. 1978, *M.N.R.A.S.*, **185**, 661.
Haynes, R. F., Jauncey, D. L., Lerche, I., and Murdin, P. G. 1979, *Australian J. Phys.*, **32**, 43.
Haynes, R. F., Lerche, I., and Murdin, P. 1980, *Astr. Ap.*, **87**, 299.
Hoffman, J. A., Marshall, H. L., and Lewin, W. H. G. 1978, *Nature*, **271**, 630.
Jones, C., Giacconi, R., Forman, W., and Tananbaum, H. 1974, *Ap. J.* (*Letters*), **191**, L71.
Kaluzienski, L. J., and Holt, S. S. 1977*a*, *IAU Circ.*, No. 3099.
———. 1977*b*, *IAU Circ.*, No. 3106.
———. 1977*c*, *IAU Circ.*, No. 3108.
———. 1978, *IAU Circ.*, No. 3171.
———. 1979, *IAU Circ.*, No. 3320.
Kaluzienski, L. J., Holt, S. S., Boldt, E. A., and Serlemitsos, P. J. 1976, *Ap. J.* (*Letters*), **208**, L71.
Katz, J. I. 1973, *Nature Phys. Sci.*, **246**, 87.
Lamb, F. K., Fabian, A. C., Pringle, J. E., and Lamb, D. Q. 1977, *Ap. J.*, **217**, 197.
Lewin, W. H. G., *et al.* 1976*a*, *Ap. J.* (*Letters*), **207**, L95.
Lewin, W. H. G., Li, F., Hoffman, J. A., Doty, J., Buff, J., Clark, G. W., and Rappaport, S. 1976*b*, *M.N.R.A.S.*, **177**, 93P.
Li, F. K., and Clark, G. W. 1974, *Ap. J.* (*Letters*), **191**, L27.
Margon, B., Lampton, M., Bowyer, S., and Cruddace, R. 1971, *Ap. J.* (*Letters*), **169**, L23.
Mason, K. O., Hawkins, F. J., Sanford, P. W., Murdin, P., and Savage, A. 1974, *Ap. J.* (*Letters*), **192**, L65.
Mayo, S. K., Whelan, J. A. J., and Wickramasinghe, D. T. 1976, *IAU Circ.*, No. 2957.
Merritt, D., and Petterson, J. A. 1980, *Ap. J.*, **236**, 255.
Murdin, P., Jauncey, D. L., Haynes, R. F., Lerche, I., Nicolson, G. D., Holt, S. S., and Kaluzienski, L. J. 1980, *Astr. Ap.*, **87**, 292.
Nicolson, G. D., 1980, *IAU Circ.*, No. 3449.
Nicolson, G. D., Feast, M. W., and Glass, I. S. 1980, *M.N.R.A.S.*, **191**, 293.
Oda, M. 1977, *Space Sci. Rev.*, **20**, 757.
Oda, M., Takagishi, K., Matsuoke, M., Miyamoto, S., and Ogwara, Y. 1974, *Pub. Astr. Soc. Japan*, **26**, 303.
Parsignault, D. R., *et al.* 1976, *Ap. Space Sci.*, **42**, 175.
Primini, F. A. 1976, Ph. D. Thesis, MIT.
Rappaport, S., Clark, G. W., Cominsky, L., Joss, P. C., and Li, F. 1978, *Ap. J.* (*Letters*), **224**, L1.
Rothschild, R. E., Boldt, E. A., Holt, S. S., and Serlemitsos, P. J. 1974, *Ap. J.* (*Letters*), **189**, L13.
Rothschild, R. E., Boldt, E. A., Holt, S. S., and Serlemitsos, P. J. 1977, *Ap. J.*, **213**, 818.
Sadeh, D., *et al.* 1979, *Nature*, **278**, 436.
Spada, G., Bradt, H., Doxsey, R., Levine, A., and Rappaport, S. 1974, *Ap. J.* (*Letters*), **190**, L113.
Sutherland, P. G., Weisskopf, M. C., and Kahn, S. M. 1978, *Ap. J.*, **219**, 1029.
Tananbaum, H., Gursky, H., Kellog, E., Giacconi, R., and Jones, C. 1972, *Ap. J.* (*Letters*), **177**, L5.
Terrell, N. J. 1972, *Ap. J.* (*Letters*), **174**, L35.
Thomas, R. M., Duldig, M. L., Haynes, R. F., and Murdin, P. 1978, *M.N.R.A.S.*, **185**, 29P.
Toor, A. 1977, *Ap. J.* (*Letters*), **215**, L57.
Ulmer, M. P., Lewin, W. H. G., Hoffman, J. A., Doty, J., and Marshall, H. 1977, *Ap. J.* (*Letters*), **214**, L11.
van der Laan, H. 1966, *Nature*, **211**, 1131.
Weisskopf, M. C., and Sutherland, P. G. 1980, *Ap. J.*, **236**, 263.
Weisskopf, M. C., Sutherland, P. G., Katz, J. I., and Canizares, C. R. 1978, *Ap. J.* (*Letters*), **223**, L17.
Whelan, J. A. J., *et al.* 1977, *M.N.R.A.S.*, **181**, 259.
Wilson, A. M., and Carpenter, G. F. 1976*a*, *Nature*, **261**, 295.
———. 1976*b*, *IAU Circ.*, No. 2965.

HALE V. BRADT: Room 37–581, Center for Space Research, Massachusetts Institute of Technology, Cambridge, MA 02139

RICHARD G. DOWER: Roxbury Latin School, West Roxbury, MA 02132

EDWARD H. MORGAN: Room 37–576, Center for Space Research, Massachusetts Institute of Technology, Cambridge, MA 02139